

Scanning tunneling microscopy of atoms and charge-density waves in $1T$ -TaS₂, $1T$ -TaSe₂, and $1T$ -VSe₂

B. Giambattista, C. G. Slough, W. W. McNairy, and R. V. Coleman
Department of Physics, University of Virginia, Charlottesville, Virginia 22901
 (Received 25 April 1989; revised manuscript received 4 December 1989)

The surface atomic structure and the charge-density-wave (CDW) structure in the $1T$ phase of TaSe₂, TaS₂, and VSe₂ have been studied at 4.2, 77, and 300 K. The response of the scanning tunneling microscope (STM) to the CDW superlattice in $1T$ -TaSe₂ and $1T$ -TaS₂ is extremely strong, while in $1T$ -VSe₂ the CDW generates a much weaker response. In $1T$ -TaSe₂ and $1T$ -TaS₂ at 4.2 and 77 K the STM scans show a $\sqrt{13}\mathbf{a}_0 \times \sqrt{13}\mathbf{a}_0$ pattern characteristic of a triple- q commensurate CDW structure. The atomic lattice and CDW superlattice are simultaneously resolved, but the atomic modulation represents a small fraction of the total STM deflection leading to a substantial variation in the atomic resolution. At 300 K we continue to observe a commensurate $\sqrt{13}\mathbf{a}_0 \times \sqrt{13}\mathbf{a}_0$ CDW pattern in $1T$ -TaSe₂ while $1T$ -TaS₂ shows a modulated two-dimensional structure due to the incommensurate CDW wavelength characteristic of the nearly commensurate phase. The STM scans on $1T$ -VSe₂ show a $4\mathbf{a}_0 \times 4\mathbf{a}_0$ CDW superlattice with a pattern that reflects a triple- to double- q transition in the CDW structure and the formation of domains. In $1T$ -VSe₂ the atomic modulation is dominant with a weak superimposed modulation due to the CDW superlattice. This difference in the strength of the CDW is reflected in the z deflection of the STM and in the effective barrier height as a function of tip-to-surface distance. The STM scans and profiles of z deflection have been analyzed and compared for all three materials. Defects in the CDW structure of $1T$ -TaSe₂ and $1T$ -TaS₂ have been observed which create missing CDW maxima and a variable enhancement of the surrounding CDW maxima. These appear to result from defects in the Ta layer rather than in the surface Se or S layer. Defects in the STM scans of $1T$ -VSe₂ are very localized and appear to be associated with Se-atom vacancies in the surface layer. The STM patterns and response will be reviewed and analyzed in terms of the band structures and Fermi surfaces of the various compounds. Results are also compared to information obtained from electron diffraction.

I. INTRODUCTION

The layer-structure dichalcogenide materials¹ TaS₂ and TaSe₂ grow in several different phases depending on the coordination between the Ta and chalcogen atoms and on the number of three-layer sandwiches per unit cell. The $1T$ phase has octahedral coordination between the Ta and chalcogen atoms and has one three-layer sandwich per unit cell. The high-temperature Fermi surfaces (FS's) of the $1T$ -phase Ta-based materials exhibit a favorable nesting condition and undergo a charge-density-wave (CDW) transition at temperatures well above room temperature. At low temperatures the CDW's form a $\sqrt{13}\mathbf{a}_0 \times \sqrt{13}\mathbf{a}_0$ commensurate superlattice. Scanning tunneling microscopy (STM) scans on the $1T$ -phase Ta compounds confirm the presence of an extremely strong CDW modulation corresponding to anomalously large z deflections of 2–5 Å in the constant current mode of the STM.

$1T$ -VSe₂ is also a member of the group VB layer-structure dichalcogenides and band-structure calculations² show the high-temperature FS to be similar to that of $1T$ -TaSe₂. However, sufficient differences exist such that the CDW formation is quite different. The CDW superlattice is observed to form only below room temperature and locks into a $4\mathbf{a}_0 \times 4\mathbf{a}_0$ superlattice below ~ 80 K

rather than the $\sqrt{13}\mathbf{a}_0 \times \sqrt{13}\mathbf{a}_0$ superlattice observed in $1T$ -TaSe₂. Electron and neutron diffraction experiments^{3,4} on stoichiometric $1T$ -VSe₂ detect two phase transitions, a second-order transition at 110 K and a first-order transition at ~ 80 K.

The above results suggest that observation of the CDW modulation in $1T$ -VSe₂ by STM will be considerably different than that observed for $1T$ -TaSe₂ and $1T$ -TaS₂. The STM scans at 77 and 4.2 K confirm this conclusion and show a much larger relative atomic to CDW amplitude ratio for the STM z deflections. We will present these results and compare them to the STM response observed for the strong CDW modulation in the Ta compounds.

In the case of pure $1T$ -TaSe₂, an initial CDW onset occurs at ~ 600 K followed by an incommensurate to commensurate transition at 473 K. The distorted structure¹ due to the CDW formation can be described by a six-pointed "star-of-David" cluster of 13 Ta atoms as shown in Fig. 1. The displacements of the metal atoms from their regular positions lie mainly within the metal planes while the selenium-atom displacements are mainly perpendicular to these planes. The maximum displacement of either the Ta or chalcogen atoms induced by the CDW is ≤ 0.2 Å.

The CDW forms a triple- q structure with three

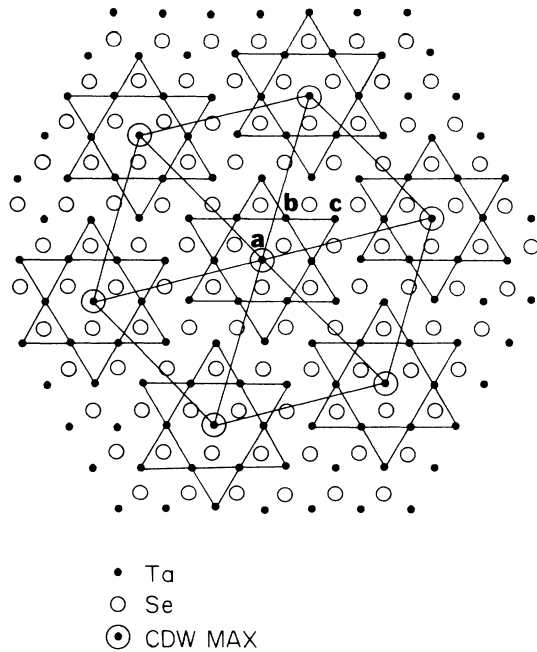


FIG. 1. Lines show the CDW supercell and the “stars of David” formed by the 13 Ta atom clusters centered on each of the CDW maxima. There is one type-*a* Ta atom, six type-*b* Ta atoms, and six type-*c* Ta atoms in each cluster. Charge is transferred by CDW formation toward the type-*a* Ta atom. The CDW supercell is rotated 13.9° from the lattice unit cell and has dimensions $\sqrt{13}\mathbf{a}_0 \times \sqrt{13}\mathbf{a}_0$.

equivalent \mathbf{q} vectors rotated by 120° in the plane of the sandwich. The low-temperature CDW structure forms a hexagonal superlattice pattern with a $\sqrt{13}\mathbf{a}_0 \times \sqrt{13}\mathbf{a}_0$ unit cell rotated 13.9° from the unreconstructed unit cell of the atomic lattice. In $1T\text{-TaSe}_2$ this is the stable structure at all temperatures below 473 K.

In $1T\text{-TaS}_2$ a CDW onset also occurs at ~ 600 K, but the incommensurate to commensurate transition occurring at lower temperatures is much more complex than that observed in $1T\text{-TaSe}_2$. A first-order transition occurs at 350 K where the triple CDW rotates by $\sim 11^\circ$ and the CDW wave vector increases in length. At ~ 150 K the CDW becomes commensurate and the rotation angle increases to 13.9° as observed in the commensurate low-temperature phase of $1T\text{-TaSe}_2$. The complex intermediate CDW phases between 150 and 350 K show hysteresis with respect to warming and cooling and several subphase geometries have been observed and identified by diffraction studies. These intermediate CDW phases are identified as two distinct nearly commensurate (NC) phases of slightly different symmetries and both have been studied by Thomson *et al.*⁵ using STM. They have been able to analyze details of the rotation and resulting domain boundaries, and to distinguish the detailed structure of these two NC phases. They have observed domain boundaries in the lower-temperature nearly commensurate *T* phase.

In previous STM studies at 77 and 4.2 K Slough *et al.*⁶ and Coleman *et al.*⁷ showed that the CDW structure

contributes an anomalously large amplitude to the STM scan in the constant current mode. Typical z deflections were in the range 2–5 Å, while the amplitude modulation contributed by the surface S or Se atoms was extremely weak.

In more recent work with STM's operating at 4.2 and 77 K we have been able to obtain STM images that give better resolution of the CDW and atomic modulations simultaneously. These results allow a careful comparison of the relative amplitude contributions in both $1T\text{-TaSe}_2$ and $1T\text{-TaS}_2$. Although the atomic modulation amplitude remains a small fraction of the total modulation, the atomic structure is clearly resolved in gray-scale images of the pure $1T$ phase crystals. The failure to detect a well-resolved atomic structure in some STM scans can be related to either surface condition, intrinsic STM deflection connected to changes in the structure of the tip, adsorbed impurities, or surface electronic structure. The observed z deflection measured in the STM scans varies from run to run and can be a sensitive function of all of the above factors. The magnitude of the observed z deflection can also be correlated with the presence or absence of zero-bias anomalies (ZBA's). However, in all cases an extremely strong corrugation at the CDW wavelength is present in the $1T\text{-TaSe}_2$ and $1T\text{-TaS}_2$ crystals and the presence of this large amplitude at the CDW wavelength can affect the resolution of the atomic corrugation. STM scans on $1T\text{-TaS}_2$ in the incommensurate phases above 150 K and in $1T\text{-TaSe}_2$ at room temperature also show substantial variation in the resolution of the atomic modulation. At higher temperatures the total z deflection is comparable to that observed at 4.2 and 77 K, but is observed to vary substantially for different crystal tip combinations. In $1T\text{-TaS}_2$ a long-range modulation of the CDW amplitude has also been observed at room temperature.

In contrast to the $1T$ phase of TaSe_2 and TaS_2 , the pure $1T$ phase of VSe_2 shows a much weaker CDW amplitude relative to the atomic modulation and good atomic resolution is maintained in all scans. In addition the STM scans at both 4.2 and 77 K show a wide variation in z deflection as well as a variation in the relative amplitudes of the three CDW components. This latter observation suggests unequal strengths for the three components of the $4\mathbf{a}_0 \times 4\mathbf{a}_0$ hexagonal superlattice which is commensurate at 80 K and below. At higher temperatures more complex incommensurate phases have been reported. The STM results at 4.2 K indicate a competition between a triple- \mathbf{q} and a double- \mathbf{q} CDW structure leading to the formation of domains with unequal CDW structures.

In this paper we present new STM images of $1T\text{-TaSe}_2$ and $1T\text{-TaS}_2$ at 4.2, 77, and 300 K along with additional analysis of the anomalously large z deflection induced by the CDW superlattice. We compare this to the CDW z deflection observed in $1T\text{-VSe}_2$ and analyze the differences in STM response. In all three cases we obtain good resolution of both the CDW and atomic modulations and present profiles and analysis of the superimposed atomic and CDW modulations.

The complete analysis of the variations in z deflection

due to the CDW structure in the pure $1T$ -phase materials should be useful for interpreting changes in the CDW structure introduced by doping with impurities. There is sufficient variation between different STM runs on the same nominally pure $1T$ -phase material that careful characterization of the standard STM images for the pure phase materials should be established before specific impurity effects on CDW amplitudes can be clearly analyzed and assigned. In the nominally pure $1T$ -phase Ta-based compounds we have observed localized defects in the CDW structure which show up as well-defined missing maxima and modified intensities in the CDW superlattice pattern. In $1T$ -VSe₂ defects identified with Se vacancies have been observed. Examples of such defects in all three $1T$ -phase materials will be discussed. We also present results of I versus V and dI/dV versus V studies at 4.2, 77, and 300 K along with analysis of possible CDW gaps and effective barrier heights.

In the case of doping with substitutional impurities replacing Ta, STM scans at room temperature on Ti_xTa_{1-x}S₂ crystals by Wu *et al.*⁸ have shown that the CDW structure becomes randomly distorted as the Ti concentration increases. They assign this random distortion of the CDW to the presence of disordered Ti sites. They also show that the average CDW wavelength increases with Ti concentration in agreement with previous electron diffraction studies.⁹

In this paper we limit our discussion to localized point defects and their effects on the local CDW amplitude in the neighborhood of the point defect. Areas with high concentrations of defects clearly show regions of CDW disorder in addition to localized defects, but these observations will be reported elsewhere.

II. EXPERIMENTAL TECHNIQUES

A. STM operation

The STM's used in the present experiments are operated in a bath of liquid nitrogen or liquid helium and are of a compact design giving high resolution. They have been operated in the constant current mode with a sensitivity that can detect a variation in z deflection as small as 0.02 Å.

The x - y translators were cut from a single block of Channel 5400 piezoelectric material and the scanning tip is placed in a collet located at the junction of the x and y arms. The scanning tip is made from Pt_{0.8}Ir_{0.2} wire, 0.5 mm in diameter. A semicircular bimorph is clamped above the x - y translator with spacers between the translator and bimorph. The sample is mounted near the front edge of the bimorph which provides the controlled z motion. The z deflection of the bimorph is regulated by means of a preamplifier and a logarithmic integrating error amplifier which controls the tip-to-sample current by measuring the voltage across a series resistor. Additional details on the construction of the liquid-nitrogen microscope have been given by Drake *et al.*¹⁰ while the liquid-helium microscope has been described by Coleman *et al.*¹¹

The x - y translator operating at 77 K has overall dimen-

sions of 2.75×2.25 cm² and provides a motion of both the x and y arms on the order of 3.3 Å/V. The maximum voltage applied is 300 V giving a maximum scan area of 1000×1000 Å². The bimorph provides a z deflection of 17.5 Å/V at 77 K and has a maximum range of 350 Å.

For operation at liquid-helium temperatures the x - y translator and bimorph have reduced overall dimensions in order to allow insertion into a liquid-helium storage Dewar or a superconducting solenoid. The x - y translator is 1.9×1.2 cm² and the semicircular bimorph has a radius of 0.75 cm. At 4.2 K the piezoelectric coefficients are reduced by a factor of 3 compared to their values of 77 K. This reduction, coupled with the smaller dimensions of the translator, limits the maximum scan area to 130×130 Å² when using a voltage range of 380 V. The bimorph provides a z deflection of 3.5 Å/V giving a maximum deflection of 70 Å.

The computer control of the STM data acquisition is accomplished by connecting the amplified output of two 12-bit digital-to-analog converter (DAC's) to the x - y piezoelectric translator. This permits scan steps as small as 0.16 Å at 77 K and 0.04 Å at 4.2 K. The z -deflection information is acquired by digitizing the z -piezo voltage using a 12-bit analog-to-digital converter (ADC) with a range of ± 10 V. The computer control improves image quality by signal averaging with 50–100 z values per (x, y) point taken in a typical scan. The time required to record a complete image is normally in the range 1–2 min.

The tunneling currents used in these experiments are in the range 1–10 nA and the bias voltage can be varied in the range 0–3 V. The layer-structure compounds covered in this paper remain metallic down to the lowest temperatures and the bias voltages are usually held in the range 1–100 mV for the STM scans with the tip positive.

B. Experimental techniques

for measuring I versus V and dI/dV versus V

The I versus V and dI/dV versus V curves were measured with the STM adjusted to a constant tunneling distance. This was usually set during the STM scan of the surface where the tunneling distance is determined by the values of I and V selected for the scan. A specific (x, y) position on the surface was then selected and the error amplifier was disengaged in order to maintain a constant voltage on the bimorph. The bias voltage for the STM was then swept by the computer in steps of 2–5 mV over the selected range of voltage and the corresponding values of I were recorded. The dI/dV (conductance) versus V curves were recorded simultaneously with an ac modulation of the bias voltage at a frequency of 1 kHz with an amplitude of 3 mV. The resulting ac current was detected with a lock-in amplifier.

C. Crystal preparation

The $1T$ -phase layer-structure crystals used in this investigation were grown by the method of iodine-vapor transport. Stoichiometric mixtures of powders were prereacted by sintering in vacuum at 900 °C for 48 h. The sintered powder was then placed in a quartz tube and

iodine vapor was condensed into the tube before sealing under vacuum. The 1*T*-phase crystals of TaSe₂ and TaS₂ were grown at temperatures above 900 °C in a temperature gradient of ~10 °C/in. for several weeks. The growth tube was then quenched in cold water to stabilize the 1*T* phase which remains stable indefinitely at room temperature. Both 1*T*-TaSe₂ and 1*T*-TaS₂ grow as shiny gold colored platelets with dimensions up to 3×3×0.2 mm³.

The 1*T*-VSe₂ crystals were grown at a growth temperature of ~770 °C in a gradient of ~15 °C/in. After a growth period of one to two weeks they were allowed to cool to room temperature without quenching since the 1*T* phase is stable at all temperatures below the growth temperature. The resulting platelets have dimensions up to 3×3×0.2 mm³ and are silvery-gray in color.

III. EXPERIMENTAL RESULTS

A. 1*T*-TaSe₂

A STM scan of 1*T*-TaSe₂ at 4.2 K recorded by computer and presented as contours of constant *z* deflection is shown in Fig. 2. The CDW charge maxima correspond to positions where there is a maximum in the local density of states (LDOS) at the Fermi level at the position of the tunneling tip and these appear as white plateaus in the STM scan. The measured spacing of the CDW maxima is 12.5±0.1 Å. The contours of constant LDOS at the Fermi level in this scan suggest very little evidence of modulation by the surface layer of Se atoms. The interstitial positions between the charge maxima show three deep minima and three saddle points symmetrically located relative to the maxima in the CDW superlattice. These contours again show little or no perturbation due to modulation arising from the surface Se-atom potentials. The pattern shows that the major spatial variation in the LDOS in this STM scan was due to the CDW su-

perlattice structure. The maximum to minimum *z* deflection for this scan was ~5 Å.

In contrast to the STM scan shown in Fig. 2 the STM scan shown in Fig. 3 clearly shows contours modified by the presence of the superimposed atomic modulation. The total *z* deflection in this case is again large at 3.1±0.2 Å with the majority fraction of 2.3±0.2 Å due to the CDW modulation and a much smaller fraction of 0.8±0.2 Å due to the atoms. Nevertheless, a gray-scale image as shown in Fig. 4(a) clearly resolves the complete atomic structure of surface Se atoms superimposed on a CDW modulation of much larger amplitude. The asymmetry of the CDW maxima reflects the phase difference between the CDW superlattice and the surface Se-atom modulations. The CDW charge maxima are centered on the 13-atom clusters of Ta atoms in the layer below the surface layer of Se atoms. The Ta atoms are displaced by $a_0/\sqrt{3}$ in lateral position from the nearest-neighbor Se atoms in the layer above. This results in a combined CDW and surface atom modulation with the asymmetry which is characteristic of all the layer-structure STM patterns^{11,12} where CDW's and surface atom modulations are simultaneously observed.

The relative strength of the atom pattern and the degree of atomic resolution are extremely sensitive to the STM response since they represent a small fraction of the total *z* deflection. The relative fraction can best be examined by comparing profiles along various directions in the STM image. Examples for 1*T*-TaSe₂ at 4.2 K are shown in Figs. 4 and 5. Figure 4(b) shows a profile recorded at 4.2 K along a path as shown in the gray-scale image of Fig. 4(a). In this case the atomic modulation is clearly resolved, but represents only a very small fraction of the total *z* deflection, ~0.2 Å out of a total of ~2 Å. A STM profile recorded from a different run and a different cleaved crystal at 4.2 K is shown in Fig. 5(b). This was recorded along the path shown in the gray-scale image of Fig. 5(a). In this case only the CDW modulation is

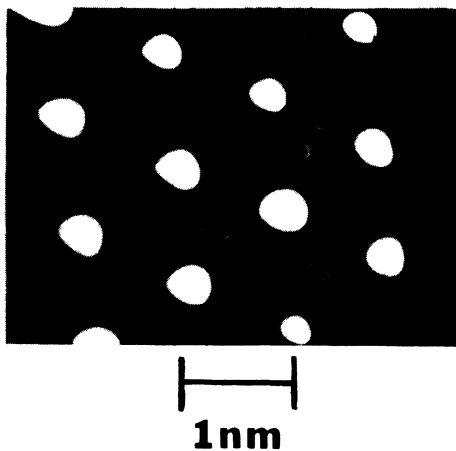


FIG. 2. STM scan at 4.2 K from the surface of a 1*T*-TaSe₂ crystal presented as contours of constant *z* deflection (constant LDOS). The contours in this STM scan detect only the CDW superlattice. ($I=2.2$ nA, $V=30$ mV.)

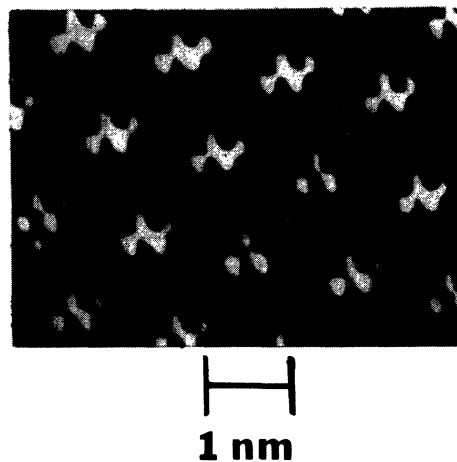


FIG. 3. STM scan at 4.2 K from the surface of a 1*T*-TaSe₂ crystal. Contours of constant *z* deflection in this case show a significant perturbation by the atomic modulation although the CDW superlattice is still dominant. ($I=2.2$ nA, $V=5$ mV.)

resolved and the atomic modulation is below the resolution limit of the STM scan.

These two profiles demonstrate how sensitive the STM resolution of the atomic modulation is to slight variations in some aspect of the STM scanning conditions when a large CDW modulation is present. This sensitivity clearly arises from the extremely small relative magnitude of the atomic modulation. Further discussion of these variations and possible sources of this variable response will be included in Sec. IV.

B. $1T\text{-TaS}_2$

The same general behavior has been observed for the STM scans on $1T\text{-TaS}_2$. However, in this case the atomic modulation by the surface S atoms, although variable, is systematically larger than observed for the Se surface atoms of $1T\text{-TaSe}_2$. Figure 6 shows two examples of STM scans on $1T\text{-TaS}_2$ taken at 77 K and recorded as contours of constant z deflection (constant LDOS). The scan shown in Fig. 6(a) shows contours completely dom-

inated by the CDW superlattice with a total z deflection of $3.9 \pm 0.4 \text{ \AA}$. The contours are slightly distorted due to the surface atom potentials, but the deep minima and saddle points generally reflect only the symmetry of the CDW superlattice. In contrast, Fig. 6(b) shows another STM scan at 77 K where the contours of constant z deflection (LDOS) strongly reflect the presence of the surface atomic potentials which cause many of the contours to close around surface atom positions. The CDW superlattice still produces an anomalous total deflection of $3.0 \pm 0.2 \text{ \AA}$. The maxima appear as white plateaus, although in this case they show strong asymmetries in shape introduced by the atomic potentials. The experimentally measured spacing of the CDW maxima is $11.9 \pm 0.2 \text{ \AA}$.

The gray-scale STM image corresponding to the contour plot of Fig. 6(b) is shown in Fig. 7(a) and detects a strong pattern of superimposed atomic and CDW modulations. The CDW maxima spaced on the $\sqrt{13}a_0 \times \sqrt{13}a_0$ superlattice are characterized by a three-atom cluster showing a slight asymmetry in z deflection. This is again a consequence of the phase shift introduced

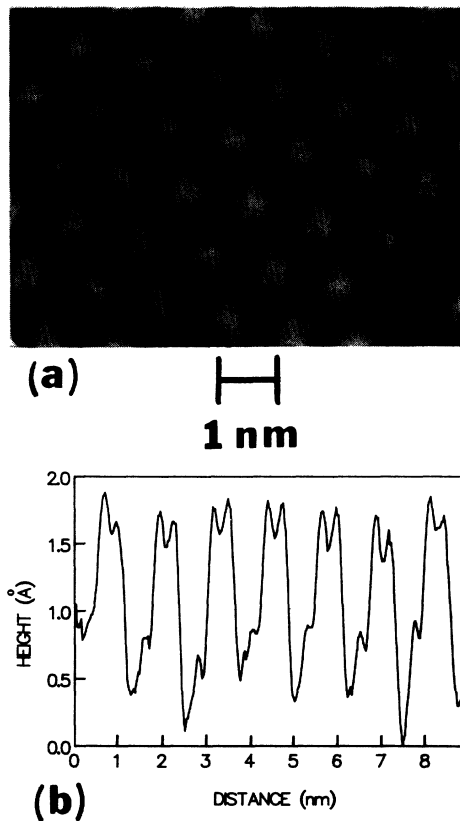


FIG. 4. (a) Gray-scale image of a STM scan on $1T\text{-TaSe}_2$ at 4.2 K. The surface Se atoms are resolved and appear as a superposition with the CDW modulation of much larger amplitude. White areas with a weak superimposed atomic modulation are centered on the CDW maxima which are displaced by $a_0/\sqrt{3}$ from the surface Se-atom positions. (b) Profile of the z deflection recorded along the track indicated in (a). The z deflection is dominated by the CDW with a very small atomic modulation.

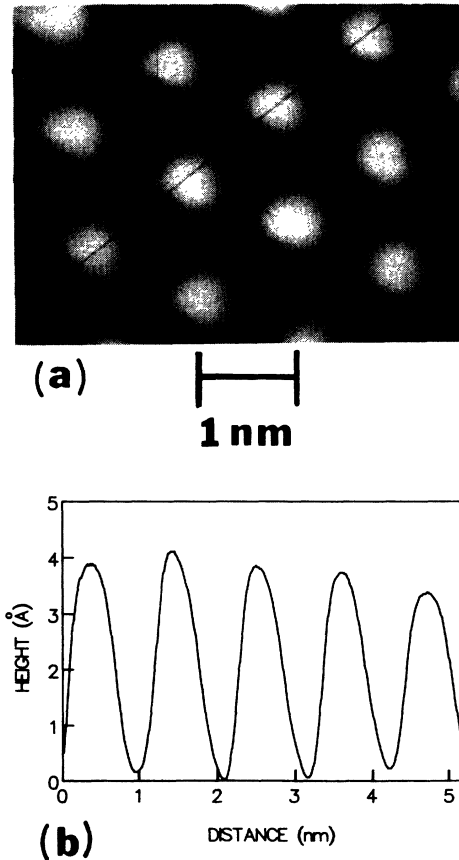


FIG. 5. (a) Gray-scale image of a STM scan on $1T\text{-TaSe}_2$ at 4.2 K which detects only the CDW superlattice. (b) The profile along the track shown in (a) shows a very strong CDW deflection of $\sim 4 \text{ \AA}$, but shows no structure due to the atomic modulation.

by the $a_0/\sqrt{3}$ displacement between the surface S-atom layer and the underlying Ta-atom layer which supports the CDW. The STM profiles obtained from this image show the clear presence of a regular atomic modulation. Figure 7(b) shows a profile recorded along the track indicated in the gray-scale image of Fig. 7(a). The atom modulation is well defined but again represents only a small fraction of the total z deflection of $\sim 2 \text{ \AA}$ along this path and is resolved at the positions of both maximum and minimum z deflections.

The variation of atomic definition in the STM scans is again related to subtle changes in the STM response in the constant current mode. The presence of the anomalously large CDW modulation as compared to the much smaller atomic modulation provides a condition in which the atomic pattern is at the limit of STM resolution. The mechanism of the anomalous CDW deflection may play a role in the observed variation of the atomic resolution

and this will be discussed in Sec. IV. Results which compare the z deflections of all of the phases of the various layer compounds exhibiting CDW's have been reviewed by Coleman *et al.*¹¹

C. 1T-VSe₂

The STM scans of 1T-VSe₂ at both 77 and 4.2 K show a $4a_0 \times 4a_0$ superlattice in the layer plane. The typical gray-scale STM images show good definition of both the atomic and CDW modulations. The total z deflection changes from run to run and has been observed to vary from 0.1 to as much as 4 Å. The typical z deflection is $\sim 0.8 \pm 0.1 \text{ \AA}$ and in all cases the atomic modulation is well resolved with no evidence of a loss of atomic modulation as occurs in the 1T-phase Ta compounds. The relative CDW to atomic modulation is also somewhat variable from run to run, but the atomic modulation represents a large fraction of the total modulation and is enhanced along with any enhancement of the CDW deflection.

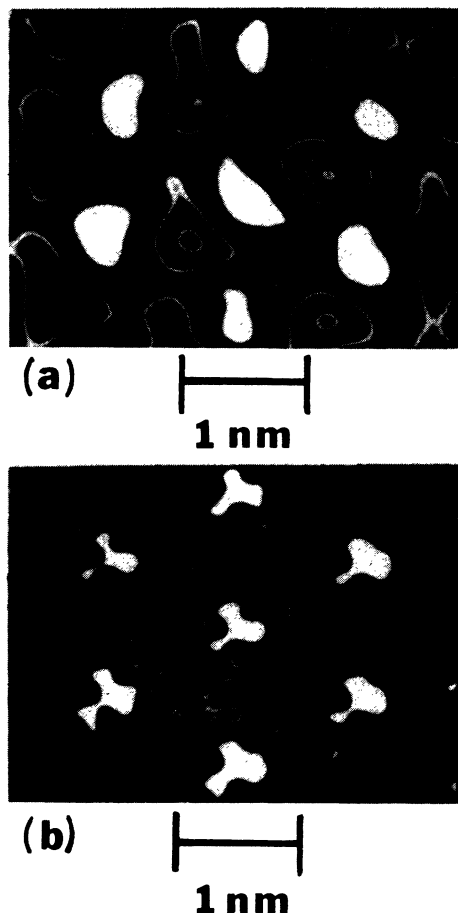


FIG. 6. (a) STM scan at 77 K from the surface of a 1T-TaS₂ crystal presented as contours of constant z deflection (constant LDOS). Contours follow the CDW superlattice with a slight distortion by the surface S atoms. ($I=2 \text{ nA}$, $V=2 \text{ mV}$.) (b) In this STM scan of 1T-TaS₂ at 77 K the contours of constant z deflection are strongly perturbed by the surface S-atom modulation. ($I=2.2 \text{ nA}$, $V=2 \text{ mV}$.) From Ref. 11.

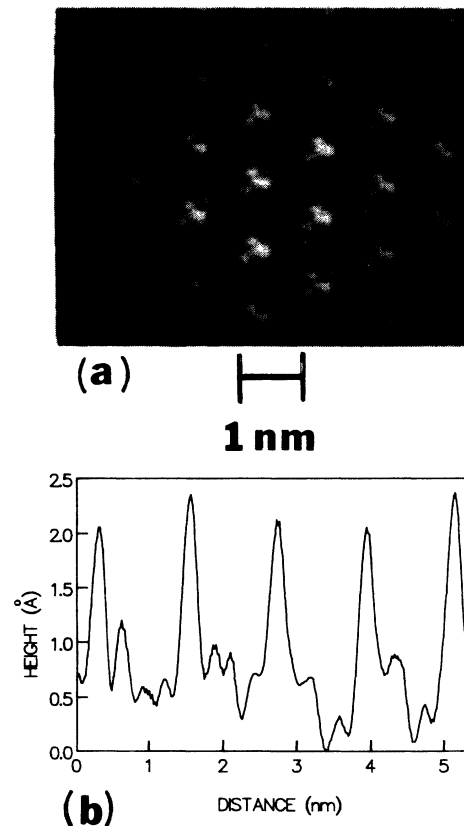


FIG. 7. (a) Gray-scale image of the STM scan on 1T-TaS₂ at 77 K used for the contour plot in Fig. 6(b). The superimposed atomic and CDW modulations are clearly resolved with an off-center three-atom cluster marking the positions of the CDW maxima. ($I=2.2 \text{ nA}$, $V=2 \text{ mV}$.) (b) Profile of the z deflection along the track shown in (a). A major fraction of the deflection occurs at the CDW wavelength with a relatively small superimposed atomic modulation. From Ref. 11.

In addition to variations in the relative amplitudes of the atomic and CDW modulations from run to run, the three components of the CDW show widely different amplitudes. This can reflect a competition between a double- and triple- q structure and hysteresis during cool down through a complex domain structure at higher temperatures. Eaglesham *et al.*¹³ have in fact concluded from electron diffraction data that at ~ 80 K the CDW adopts a double- q structure. They also observe that the crystal develops a well-defined domain structure with domain sizes ranging from 1000 \AA to a few micrometers. Details of the triple- to double- q transition and possible structures in the CDW configurations of $1T\text{-VSe}_2$ will be discussed in Sec. IV.

The gray-scale image of Fig. 8(a) shows a high magnification scan of $1T\text{-VSe}_2$ at 4.2 K. In this case the atomic and CDW modulations are comparable. The modulation enhances hexagonal groups of atoms located

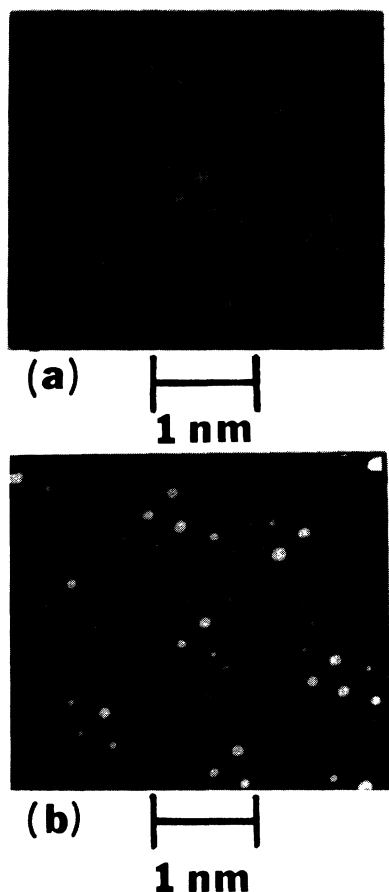


FIG. 8. (a) Gray-scale image of a STM scan on $1T\text{-VSe}_2$ at 4.2 K. The atomic and CDW modulations are of comparable magnitude. (b) Same STM scan of $1T\text{-VSe}_2$ as shown in (a) presented as contours of constant z deflection. The contours are dominated by the atomic pattern of surface Se atoms. The maxima of the CDW superlattice appear as enhanced three-atom clusters. ($I=2.2 \text{ nA}$, $V=25 \text{ mV}$.)

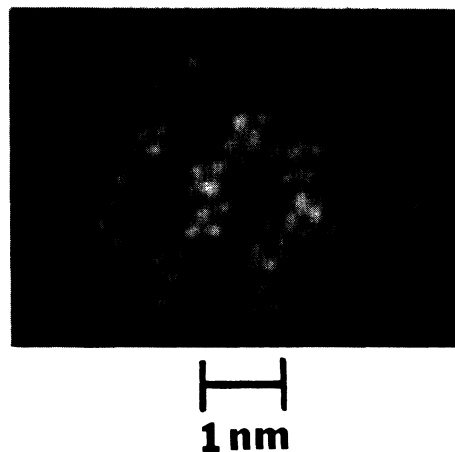


FIG. 9. Gray-scale image of STM scan on $1T\text{-VSe}_2$ at 4.2 K. The pattern shows CDW maxima separated by rather diffuse minima instead of distinct deep minima and saddle points. This pattern is characteristic of a double- q rather than a triple- q CDW structure. ($I=2.2 \text{ nA}$, $V=25 \text{ mV}$.)

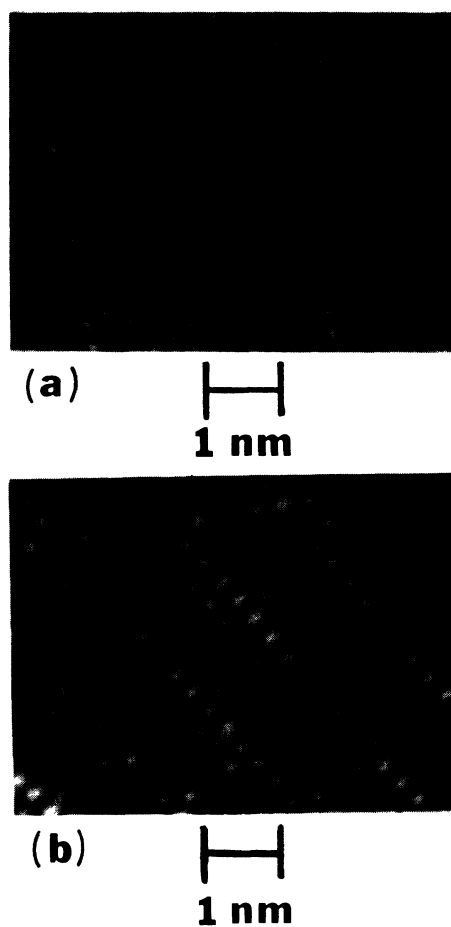


FIG. 10. Gray-scale images of STM scans on $1T\text{-VSe}_2$ showing unidirectional enhancement of the CDW pattern. (a) Scan at 4.2 K showing enhancement of two atomic rows along a single diagonal direction. ($I=2.2 \text{ nA}$, $V=25 \text{ mV}$.) (b) Scan at 77 K showing enhancement of three-atom rows along a single diagonal direction.

on a $4a_0 \times 4a_0$ superlattice, although the enhancement is both slightly asymmetric as well as diffuse. The corresponding contour plot is shown in Fig. 8(b). The CDW maxima show up as groups of three individually enhanced atoms while the detailed contours of constant z deflection generally follow the modulation produced by the individual atomic potentials. The groups of three enhanced atoms in Fig. 8(b) form a hexagonal superlattice. The gray-scale images of $1T\text{-VSe}_2$ at 4.2 K show superlattice modulation patterns that exhibit symmetries characteristic of both double- and triple- q structures. The uniform triple- q CDW structure would be characterized by the usual pattern of deep minima and saddle points within the interstitial regions of each rhombohedral unit cell of the hexagonal superlattice. When the double- q structure is dominant the minima become broadened and shift toward the center of the unit cell giving only a large diffuse minima centered within each unit cell of the superlattice as shown in Fig. 9. This shift in the symmetry of the STM pattern is consistent with a shift in charge distribution associated with the double- q versus triple- q CDW structure.

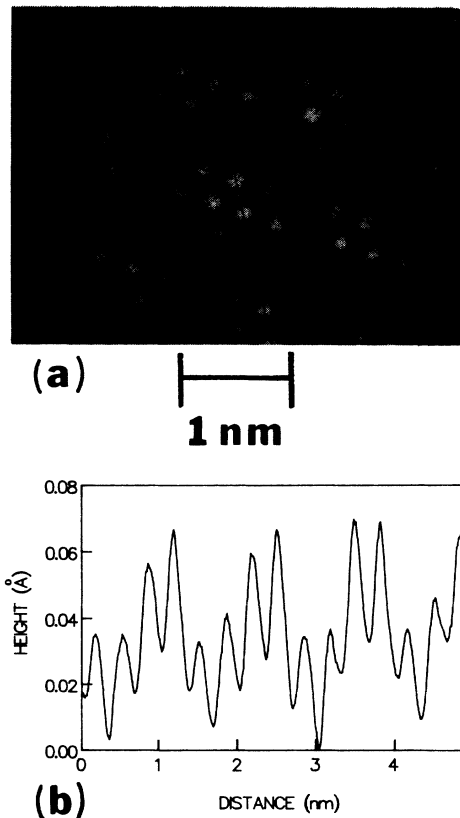


FIG. 11. (a) Gray-scale image of $1T\text{-VSe}_2$ at 4.2 K showing well-defined groups of seven surface Se atoms marking the positions of the CDW maxima. ($I=2.2$ nA, $V=25$ mV.) (b) Profile of the z deflection along one of the diagonal tracks in (a). All of the profiles show an extremely small modulation of ~ 0.07 Å which is dominated by the atomic modulation at a wavelength of $4a_0$.

The superlattice pattern detected by the STM can also show a number of other variants. For example, as shown in the lower magnification gray-scale images of Fig. 10 the STM scans can show a strong modulation by the CDW in one direction while the other two equivalent directions oriented at 120° show much weaker modulations. Figure 10(a) shows a STM scan at 4.2 K where one diagonal direction shows a strong enhancement extending over two rows of atoms while the other two directions show a much weaker enhancement. Figure 10(b) shows a similar result obtained with a STM scan at 77 K where a strong CDW enhancement extends over three rows of atoms in one direction while the other equivalent directions show weak enhancements. This change in the relative enhancement of the individual q vectors along with the changes in total z deflection indicate substantial variation in the detailed CDW formation and STM response in $1T\text{-VSe}_2$.

The profiles of the STM scans on $1T\text{-VSe}_2$ generally show a pattern of well-defined atoms with the CDW modulation superimposed as a smooth undulation with a wavelength of $4a_0$. However, the total z deflection ob-

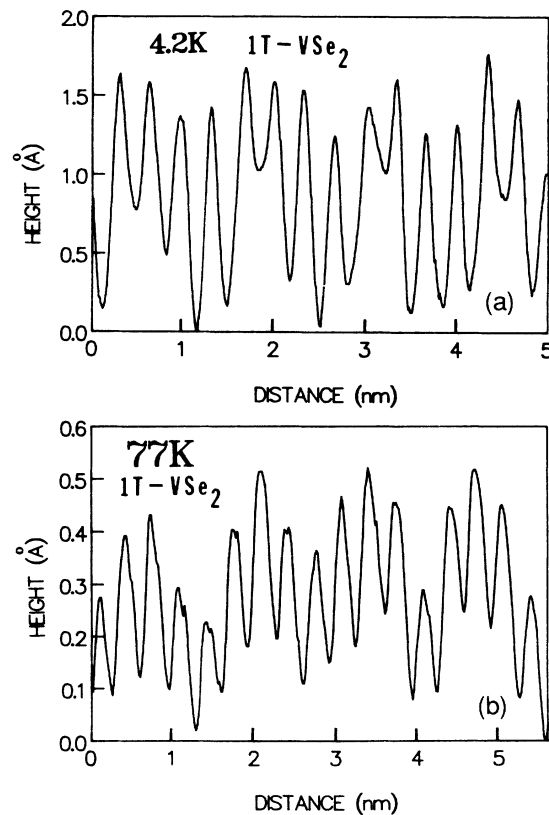


FIG. 12. Profiles of representative STM scans on $1T\text{-VSe}_2$ demonstrating the wide variation in total z deflection observed for different runs and different crystals. (a) Profile of a scan at 4.2 K with a maximum z deflection of ~ 1.8 Å. ($I=2.2$ nA, $V=25$ mV.) (b) Profile of a scan at 77 K with a maximum z deflection of ~ 0.5 Å. ($I=2$ nA, $V=23.3$ mV.)

served can vary by at least an order of magnitude without changing the appearance or lateral resolution of the STM image. A typical profile obtained at 4.2 K is shown in Fig. 11(b) for the diagonal track running from lower left to upper right in Fig. 11(a). The track passes through the CDW maxima and the profile is dominated by the atomic modulation with the superimposed long-range CDW modulation of wavelength $4a_0$. The total z deflection is extremely small with a value of 0.07 \AA , the smallest ever observed. Profiles along the two other tracks in Fig. 11(a) show a similar result. A much larger total z deflection of $\sim 1.8 \text{ \AA}$ was observed for the STM scan profile recorded at 4.2 K on another crystal as shown in Fig. 12(a) while a third crystal run at 77 K showed an intermediate total z deflection of $\sim 0.5 \text{ \AA}$ as shown in the scan profile of Fig. 12(b). This variation in z deflection can be related to the very rapid variation of an effective barrier height as a function of tunneling distance observed in $1T\text{-VSe}_2$. Fur-

ther results and analysis on this point are included in Sec. III F below.

D. CDW defects

The STM has the potential to detect a variety of defects on an atomic scale and examples have been reported for surface atom vacancies⁶ and surface adatoms.¹⁴ In the present studies of the $1T$ -phase crystals the surface atom patterns have appeared to be perfect in most cases where the surface atoms are well resolved. However, in all three $1T$ -phase crystals studied, localized defects in the CDW pattern have been observed. These have a common characteristic in that they often appear as a deficit in the LDOS which would have been associated with the CDW modulation. This produces a strong local minimum in the z deflection which often appears as a "black hole" in the gray-scale images. However, in some cases a localized enhancement of the CDW maxima is also observed on surrounding CDW maxima. In $1T\text{-VSe}_2$ a Se-atom vacancy may also be associated with the defect.

1. $1T\text{-TaSe}_2$

An example for $1T\text{-TaSe}_2$ at 4.2 K is shown in Fig. 13(a). This gray-scale scan resolves only the CDW modulation and shows several such defects localized at the positions of the CDW maxima. Adjacent CDW maxima appear to be slightly enhanced, but in general the surrounding CDW maxima are remarkably unperturbed. The atomic modulation was not detected as confirmed in the higher magnification contour scan of Fig. 13(b). The maxima, deep minima, and saddle points reflect only the CDW pattern with a spacing of $12.6 \pm 0.3 \text{ \AA} = \sqrt{13}a_0$.

2. $1T\text{-TaS}_2$

In the case of $1T\text{-TaS}_2$ similar defects corresponding to missing CDW maxima have been observed at 77 K as shown to the left in Fig. 14(a). In this case the surface atom pattern is also well resolved and no evidence of missing surface atoms can be seen near the missing CDW maximum. Figure 14(b) shows a profile through the defect and modulation by the surface atoms is uninterrupted while the CDW enhancement is absent. The adjacent CDW maxima again show a slight perturbation in height, as was observed for the $1T\text{-TaSe}_2$ defects, but the major defect in the CDW pattern remains remarkably localized.

A second example of defects in the CDW superlattice of $1T\text{-TaS}_2$ is shown in the STM scan of Fig. 15. The CDW superlattice is clearly resolved with little or no contribution from the atomic modulation. The image was recorded in the commensurate phase at 153 K and gives a very large maximum z deflection in the range of $\sim 4 \text{ \AA}$. The defects in the CDW superlattice pattern are observed in a region of the crystal surface showing an irregular pattern of CDW maxima suggesting some type of disorder in the three-atom layer sandwich supporting the CDW. Associated with these local domains are two distinct types of defects involving a symmetric cluster of seven CDW maxima.

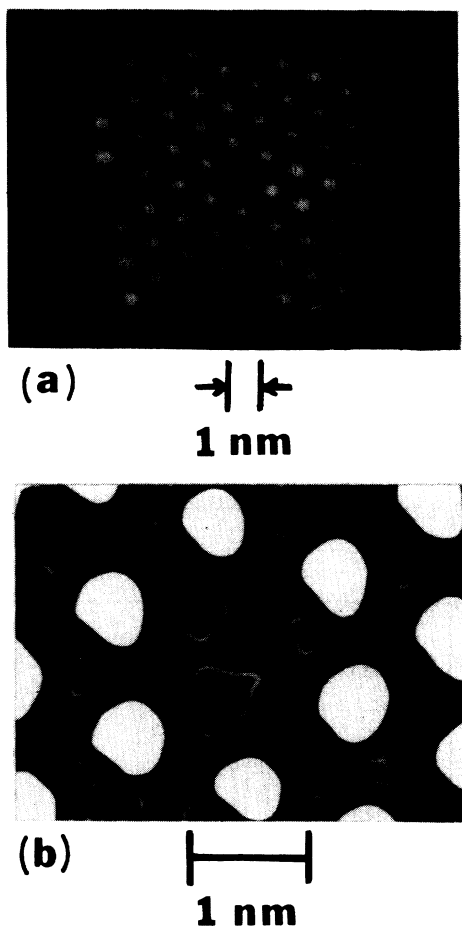


FIG. 13. STM scans on $1T\text{-TaSe}_2$ at 4.2 K showing the presence of defects in the CDW superlattice. (a) Gray-scale image showing missing CDW maxima. Pattern is totally dominated by the CDW superlattice. (b) Contour plot of the STM scan shown in (a). Contours confirm the dominance of the CDW superlattice with the region of the missing CDW maximum showing a minimum and relatively uniform z deflection in the central region. From Ref. 11.

In the lower section of the scan two defects are observed in which the center CDW maximum is missing and the six surrounding maxima are enhanced. As shown in the profile of Fig. 16(a) this enhancement of the CDW maxima is on the order of $\sim 1 \text{ \AA}$ relative to the surrounding CDW maxima and must represent a strong perturbation of the charge transfer and LDOS in the 13-atom clusters contributing to each of these CDW maxima.

In addition to the two defects discussed above at least three others are characterized by a "black hole" indicating a missing CDW maximum, but these do not exhibit the strongly enhanced ring of surrounding CDW maxima. Figure 16(b) shows the profile recorded along a track through one of these defects. The CDW maxima surrounding the defect contribute approximately the same z deflection as observed for other nearby CDW maxima. However, the missing CDW maximum shows a deeper minimum resulting in an overall minimum to maximum z deflection of $\sim 4 \text{ \AA}$, the same as observed in the defects discussed in Fig. 13.

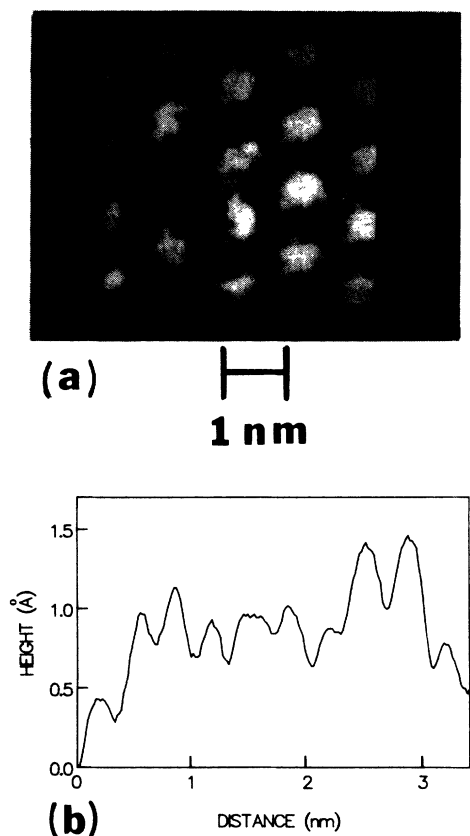


FIG. 14. (a) Gray-scale image of a STM scan on $1T\text{-TaS}_2$ at 77 K showing a missing CDW maximum. In this case the surface S atoms are resolved within the region of the missing maximum. (b) Profile of the z deflection across the center of the defect region shows a continuous modulation at the atomic wavelength. The defect does not appear to involve surface S atoms. ($I=2.2 \text{ nA}$, $V=25 \text{ mV}$.)

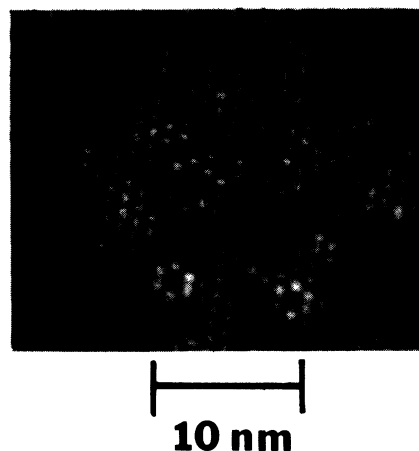


FIG. 15. Gray-scale image of a STM scan on $1T\text{-TaS}_2$ at 153 K. A number of defects involving missing CDW maxima are observed. Several of these involve enhancement of the surrounding CDW maxima while others do not show this enhancement. ($I=3 \text{ nA}$, $V=47 \text{ mV}$.)

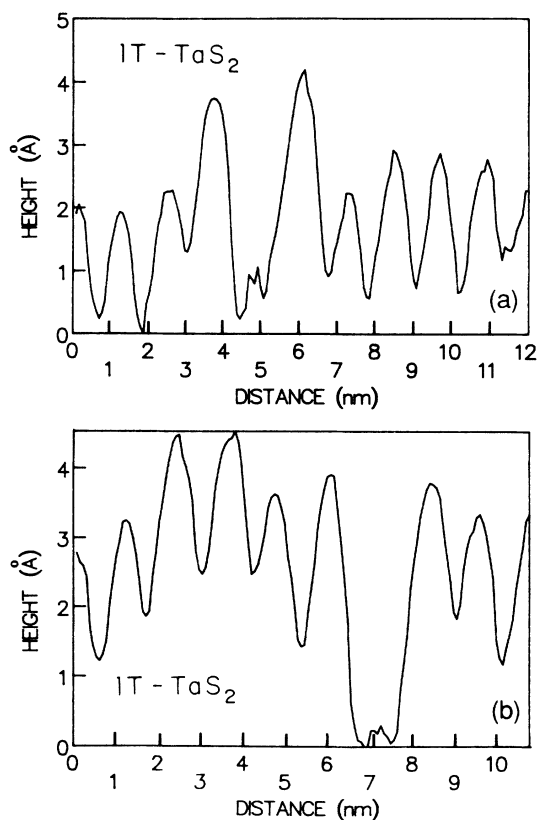


FIG. 16. Profiles of z deflection along tracks through the CDW defects shown for $1T\text{-TaS}_2$ in Fig. 15. All of the missing CDW maxima show a deep minimum giving a total relative z deflection of $\sim 4 \text{ \AA}$ with a small structure of atomic dimensions at the minimum. (a) Profile of defect with enhanced CDW maxima surrounding the missing one. (b) Profile of defect without localized enhancement of the surrounding maxima.

The cause of the CDW defects shown above would seem to be in the Ta layer of atoms since the defects represent rather drastic perturbations of the LDOS associated with the Ta d electrons participating in the CDW. Either substitutional impurity atoms or vacancies in the cluster of 13 Ta atoms associated with each CDW maximum could distort the charge transfer within the 13-atom cluster. The precise form of the defect and associated charge distribution would then depend on the number and position of the missing or substituted atoms in each 13-atom cluster. A range of different defect profiles would then be expected for random defects in the Ta layer of atoms, as is observed. $1T$ -VSe₂ also shows a similar type of CDW defect, but variations suggest subtle differences connected with the different CDW structure in $1T$ -VSe₂.

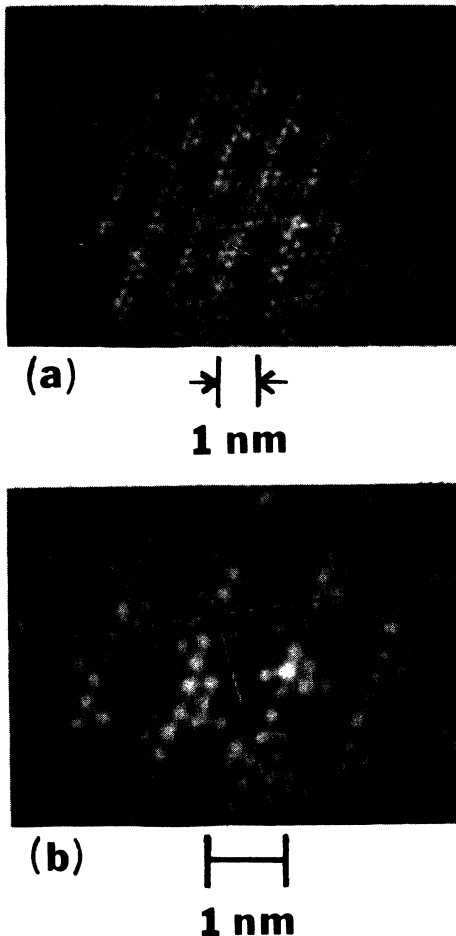


FIG. 17. Gray-scale images of STM scans on $1T$ -VSe₂ at 4.2 K showing defects in the pattern of surface Se atoms. The defects in this case are associated with missing surface Se atoms and do not have a specific correlation with the CDW superlattice. (a) Large area scan showing a number of distributed defects. Three defects in the upper half of scan are marked by localized black holes. (b) Magnified scan of two close defects near the CDW maxima. ($I=2.2$ nA, $V=25$ mV.)

3. $1T$ -VSe₂

Figure 17(a) shows a STM scan of $1T$ -VSe₂ at 4.2 K where three separate "black hole" defects are located in the upper half of the scan. The one on the right occurs at a position close to a CDW maximum while the two on the left are slightly off the maxima. These defects are more localized than observed for $1T$ -TaSe₂ and $1T$ -TaS₂ and are only slightly wider than a single atom. They could result from surface Se-atom vacancies in this case since the atomic modulation is a larger fraction of the total modulation. The surface Se atoms may also participate to a greater extent in the charge transfer associated with the CDW.

A magnified scan of the two close defects is shown in Fig. 17(b) along with profiles in Fig. 18(a) which correspond to the two scan paths intersecting the defects. These scan paths emphasize the atomic modulation of ~ 1 Å while the defect represents a tip excursion of practically 4 Å. For comparison Fig. 18(b) shows a profile

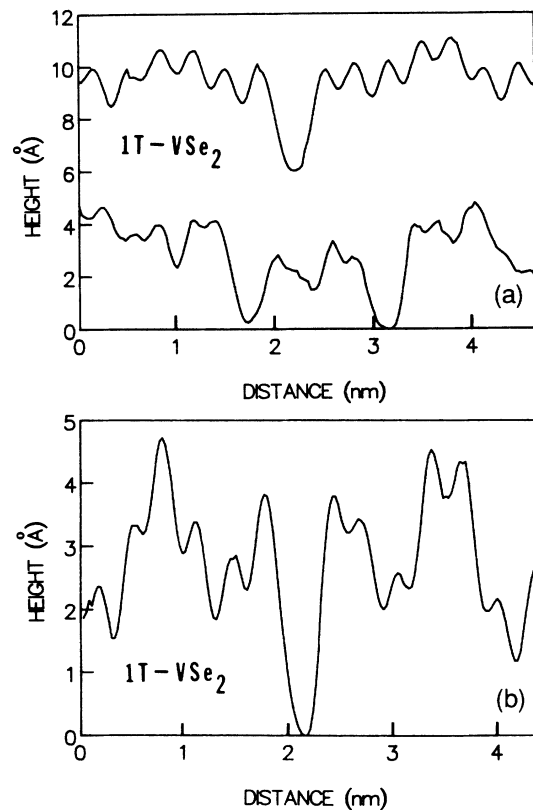


FIG. 18. (a) Profiles of the z deflections observed along tracks shown in STM scan of Fig. 17(b). Upper profile corresponds to the nearly horizontal track. Lower profile corresponds to the nearly vertical track. Both profiles show a dominant modulation at the atomic wavelength with an enhanced minimum at the position of the defect. (b) Profile of z deflection through the defect in the upper right-hand section of Fig. 17(a) demonstrating the large localized deflection associated with the defect.

which crosses the CDW maxima as well as minima and also includes a defect. The maximum to minimum CDW structure is ~ 3 Å while the defect again produces a 4-Å-deep hole with an absolute minimum in z deflection. The profile clearly shows that the defect has removed the LDOS associated with both the atomic and CDW modulations causing the tip to make a very close approach to the surface.

E. Measurements of I versus V and dI/dV versus V

The STM's have been used to obtain characteristic I versus V and dI/dV versus V curves in the range 0 to ± 1.0 V for all three 1T-phase compounds discussed above. Values of the CDW gaps have been estimated from changes of slope observed in the characteristic curves.

In the case of 1T-TaSe₂ at 4.2 K I versus V curves show an initial Ohmic region followed by a strong nonlinear behavior at voltages above ~ 150 mV. Experimental curves of I versus V and dI/dV versus V for 1T-TaSe₂ at 4.2 K are shown in Figs. 19(a) and 19(b). The nonlinear onset is rather broad and may suggest the presence of a distribution of CDW gaps in the range of 150–180

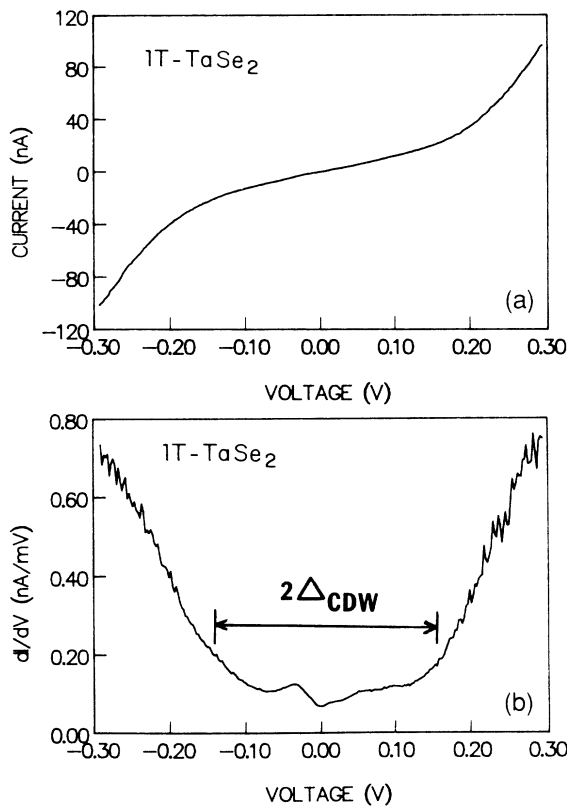


FIG. 19. (a) I vs V measured at 4.2 K on a crystal of 1T-TaSe₂. A strong nonlinear increase in current occurs near ± 150 mV indicating the possible effect of the CDW gap. (b) dI/dV vs V curve corresponding to the I vs V curve of (a). A weak zero-bias anomaly is observed.

mV. Previous tunneling measurements by Noutomi *et al.*¹⁵ with fixed 1T-TaSe₂-Al₂O₃-Al tunnel junctions estimated 2Δ at 4.2 K to be in the range 400–500 mV. The present measurements suggest 2Δ to be below this range and not greater than 300 mV.

In addition to the nonlinear behavior associated with the CDW gap, a structure associated with a zero-bias anomaly is often observed with a variable magnitude from sample to sample. The conductance curve of Fig. 19(b) shows a small ZBA in the bias range below 50 mV while other specimens can show stronger ZBA's extending up to ~ 100 mV. These do not appear to be associated with the CDW structures, but are apparently due to geometrical asymmetries or contamination effects involving the specific tunneling tip and tip-surface interactions. The presence of a ZBA is emphasized in plots of dynamic resistance versus V and an example of a large ZBA in 1T-TaSe₂ is shown in Fig. 20. The ZBA gives a strong resistance maximum at zero bias corresponding to substantial backscattering of the tunneling electrons near zero bias.

The I versus V data on 1T-TaS₂ at 4.2 K also indicate a gap of $\Delta \simeq 150$ mV as shown in the curve of Fig. 21(a). A well-defined but broadened onset of enhanced current flow is observed in the bias range above 150 mV. The ZBA's observed in 1T-TaS₂ at 4.2 K are also quite large as shown in the conductance curve of Fig. 21(b). In this case the ZBA is also directly detected in the I versus V curve near zero bias where it contributes a well-defined reduction in slope as evident in Fig. 21(a).

At 77 K both 1T-TaSe₂ and 1T-TaS₂ show the onset of a strong nonlinear current rise at a bias voltage of ~ 150 mV with a general broadening and smoothing of the characteristic tunneling curve. This is probably associated with thermal broadening in the tunneling density of states or thermal fluctuations of the CDW. Both 1T-TaSe₂ and 1T-TaS₂ show very broadened nonlinear I versus V curves at 300 K and the CDW gaps do not contribute sufficiently localized structure for analysis. The tunneling results obtained by Noutomi *et al.*¹⁵ with fixed

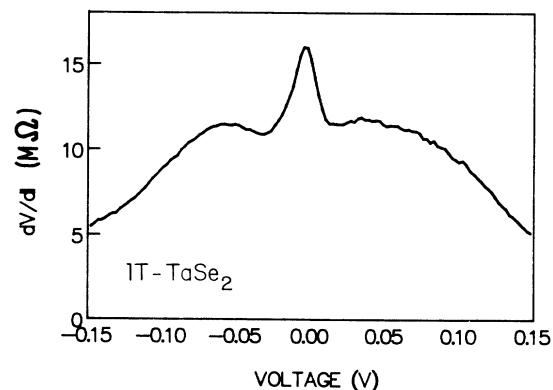


FIG. 20. dV/dI vs V measured at 4.2 K on a crystal of 1T-TaSe₂ demonstrating the strength of the positive zero-bias anomaly with a width of ~ 50 mV.

junctions suggested that between 4.2 and 300 K the CDW gap in $1T\text{-TaSe}_2$ remained constant while the CDW gap in $1T\text{-TaS}_2$ decreased rapidly above 100 K. We are unable to confirm this in our experiments since the I versus V curves of both $1T\text{-TaSe}_2$ and $1T\text{-TaS}_2$ show equally large broadening effects at 300 K.

In the case of $1T\text{-VSe}_2$ and I versus V curves at 4.2 K do not show sharp breaks in slope that can be associated with the CDW gap. A zero-bias anomaly is again present in the conductance curves and these extend up to ~ 50 mV. Above 50 mV the conductance curves can also show a peak followed by a secondary minimum at 200–300 mV. This behavior is not explained, but may be related to rapid changes in effective barrier height which can be observed when the tunneling distance is increased.

Preliminary data suggest that the presence of a ZBA is correlated with an enhanced z deflection in the STM scans. This is particularly true in the $2H$ -phase layer compounds where the intrinsic z deflection is much smaller than in the $1T$ -phase compounds. In the $1T$ -phase compounds the barrier generally remains low at high bias voltages as discussed further in Sec. III F below.

However, the barrier does increase at higher bias voltages and the z deflection of the STM image scan shows a corresponding decrease. The relative amplitudes of the CDW and atomic modulations do not appear to be influenced by the presence of ZBA's, the specific bias voltage, or the effective barrier height at a given voltage. Only the total z deflection shows a correlation. Any enhancement mechanisms not associated with the CDW structure itself appear to enhance the CDW and atomic modulations equally. For example, in $1T\text{-VSe}_2$ the STM amplitudes can vary by an order of magnitude while the atomic modulation relative to the CDW modulation remains approximately the same (see Fig. 12).

In addition the I versus V and the effective barrier height versus V results do not depend on whether the STM tip is located at an atom, a CDW maximum, or a CDW minimum. The characteristic tunnel curves are essentially the same at closely adjacent positions within a 10-\AA radius on the surface. Most of the STM scans shown here are taken in the bias range 2–25 mV corresponding to fairly low barrier heights and larger total z deflections. The latter contribute to better image definition.

F. Barrier heights

The typical values of current and bias voltage used for the STM scans in these studies are 1–3 nA and 5–25 mV. An effective tunnel barrier height can be calculated by measuring dI/dz at a given current and using the low voltage approximation given in Eqs. (1)–(4). dI/dz can be measured by setting the current and voltage of the STM, applying an ac voltage to the bimorph in order to produce a calibrated amplitude Δz , and measuring ΔI with a lock-in amplifier tuned to the bimorph modulation frequency. The effective barrier height ϕ is then calculated using Eq. (4):

$$I = e^{-A\phi^{1/2}z}, \quad (1)$$

$$\ln I = -A\phi^{1/2}z + \text{const}, \quad (2)$$

$$\phi = A^{-2} \left[\frac{d \ln I}{dz} \right]^2 \quad (3)$$

with ϕ in volts and z in angstroms. With $A \approx 1.025$

$$\phi = 0.95 \left[\frac{d \ln I}{dz} \right]^2. \quad (4)$$

The above expressions are approximately valid only for $V \ll \phi$ and for parallel plane electrodes. Therefore applications to the STM data provide only a rough estimate of the barrier height behavior. By setting the dc current at a constant value and measuring dI/dz at various dc voltages in the range 0–500 mV the barrier height as a function of tunneling distance z can be measured. At constant dc current z increases as voltage bias increases, but no absolute values of z can be determined at present. The change in distance over the range 5–500 mV is estimated to be $\sim 3 \text{ \AA}$.

Results of barrier height versus bias voltage for $1T\text{-}$

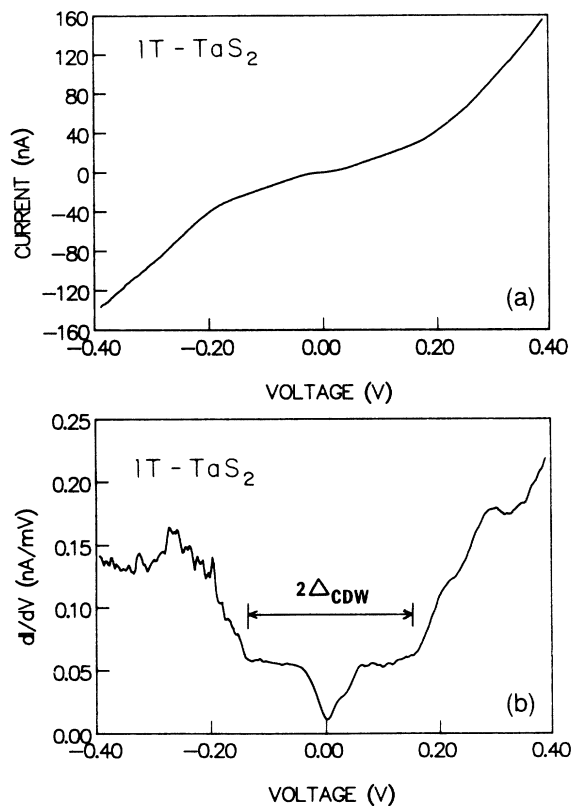


FIG. 21. (a) I vs V curve measured at 4.2 K on a crystal of $1T\text{-TaS}_2$. A strong nonlinear increase in current is observed above ~ 150 mV indicating a possible CDW gap. (b) dI/dV vs V showing a sharp increase in conductance at ~ 150 mV. A substantial zero-bias anomaly is also observed.

TaSe₂ and 1T-VSe₂ at 4.2 K are shown in Figs. 22(a) and 22(b). These results suggest that the effective barrier can change rapidly as the bias voltage (tunnel gap) is increased. This result is consistent with the z deflection measured from the STM scans at different bias voltages for constant current. At low bias voltage a large z deflection is observed and this can decrease significantly at higher bias voltage giving a rapid increase in effective barrier height. In 1T-TaSe₂, with a very strong CDW, this decrease is slower and the barrier height remains relatively low. However, in 1T-VSe₂, with a weak CDW, the rise in effective barrier height is faster and reaches a much higher value. The source of the large STM z deflection observed in CDW materials will be discussed further in Sec. IV B. The behavior of barrier heights, ZBA's, and energy gaps have been studied for a wide range of layer-structure compounds and these results will be presented in detail in another publication. The main points associated with the STM images discussed in this paper are not strongly influenced by the variations observed in the characteristic tunnel curves as a function of

voltage. The tunnel curves appear to be much more sensitive to the detailed tunneling processes, junction spacing, and tip condition than the images.

IV. DISCUSSION

A. Electronic structure of the 1T-phase crystals

The band structures of the undistorted 1T-phase compounds have been calculated by Mattheiss¹⁶ using augmented plane-wave (APW) methods, by Myron and Freeman¹⁷ using Korringa-Kohn-Rostoker (KKR) methods, and by Woolley and Wexler² using the layer method. Fermi-surface cross sections have been worked out in some detail for the 1T phase of TaS₂, TaSe₂, and VSe₂ by Woolley and Wexler.² The high-temperature Fermi surfaces of these three compounds are similar except that the selenides show greater curvature in the k_z direction and have a pancake-shaped region of electrons around the center of the zone at Γ while in 1T-TaS₂ this band is unoccupied.

Smith *et al.*¹⁸ have calculated a model band structure for the CDW phase of 1T-TaS₂, but a similar model for 1T-TaSe₂ has not been developed. They calculate rather large charge transfers between Ta atoms during CDW formation in 1T-TaS₂, and this will be discussed in Sec. IV A 1 below. Since both 1T-TaS₂ and 1T-TaSe₂ have similar high-temperature Fermi surfaces and form the same reduced Brillouin zone (BZ) due to the $\sqrt{13}a_0 \times \sqrt{13}a_0$ superlattice, large charge transfers may also occur in 1T-TaSe₂. A very large CDW amplitude is certainly observed for both materials in the STM scans suggesting a similarity in the major FS reconstruction and associated modification in the LDOS. However, the detailed charge density rearrangement on the 13-atom clusters may not be the same for the two materials. In addition, the low-temperature conductivity of 1T-TaSe₂ is much greater, consistent with extra electrons from the original high-temperature pancake and possible differences in the refolded band structure.

The FS reconstruction in 1T-VSe₂ can be expected to be substantially different. Although the high-temperature FS is very similar to that of 1T-TaSe₂, the hybridization between the d and p bands is sufficient to cause a completely different CDW superlattice of $4a_0 \times 4a_0 \times 3c_0$ to form. The band folding and FS reconstruction can therefore be expected to show major differences from those found in the 1T Ta-based compounds. No detailed calculations for the CDW phase in 1T-VSe₂ have been carried out, but the STM scans show a relatively weak CDW amplitude and suggest a much smaller charge transfer involved in the CDW and less modification in the LDOS. The details of the high-temperature band structure will be summarized in Sec. IV A 3. Further details can be found in Ref. 9.

1. 1T-TaS₂

The distorted structure in 1T-TaS₂ due to the CDW is represented by the "star-of-David" atomic arrangement

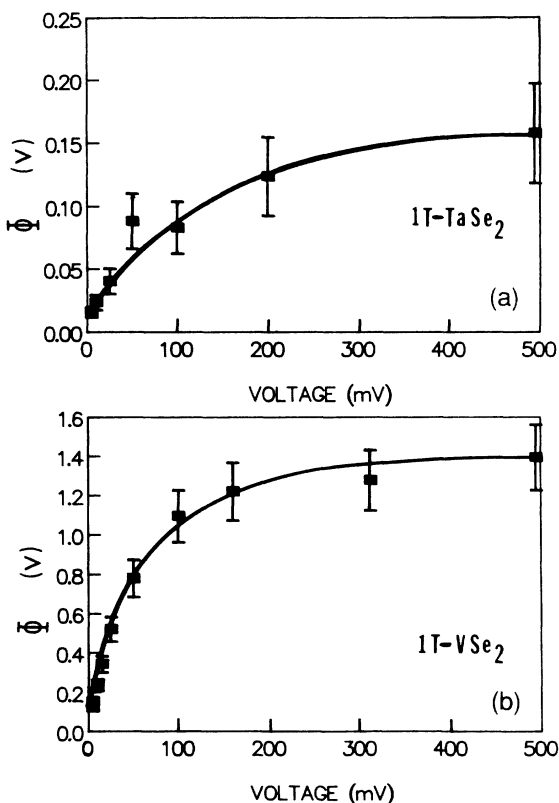


FIG. 22. Effective barrier height as function of voltage measured at 4.2 K. The barrier height is determined by measuring dI/dz and using Eq. (4). In this set of experiments increasing voltage corresponds to increasing distance between the tip and surface. (a) For 1T-TaSe₂ the barrier height is observed to saturate at a relatively low value of $\phi \approx 0.15$ V. (b) For 1T-VSe₂ the barrier height rises rapidly to a fairly high value and saturates at $\phi \approx 1.4$ V.

as was shown in Fig. 1. There are three inequivalent types of Ta atoms labeled a , b , and c in Fig. 1. Smith *et al.*¹⁸ use the band-structure results developed by Mattheiss¹⁶ and by Doran and Woolley¹⁹ as a starting point for their model of the CDW phase and adjust the model to interpret data from angle-resolved photoemission spectroscopy. Their analysis shows a major distortion of the band structure in which the d band derived from the Ta atoms collapses into three subband manifolds separated by gaps. The 13th electron resides in a very narrow band and can lead to a Mott-Anderson transition associated with the resistance rise observed¹⁸ in the liquid-helium temperature range for $1T\text{-TaS}_2$.

In the $\sqrt{13}a_0 \times \sqrt{13}a_0$ unit cell the three types of atoms a , b , and c are in the proportion 1:6:6. The atom-by-atom decomposition of the density of states (DOS) gives the total number of occupied d electrons per atom, on each type of atom. For $1T\text{-TaS}_2$ these calculated numbers are $n_a = 1.455$, $n_b = 1.311$, and $n_c = 0.611$, which indicate charge transfers involving a large fraction of an electron per atom, consistent with a large electron condensation into the CDW. The model calculation indicates that the CDW's have a fairly uniform amplitude within the seven-atom cluster centered on the a -type atom, while the amplitude decreases strongly in the interstitial regions near the c -type Ta atoms. Both the large calculated electron transfer and the fairly good FS nesting expected from the high-temperature FS topology would suggest a strong CDW amplitude. Therefore the LDOS at the Fermi level can be expected to show spatial modulation at the CDW wavelength.

2. $1T\text{-TaSe}_2$

The FS modifications in the CDW phase of $1T\text{-TaSe}_2$ have not been studied in any detail and model calculations have not been carried out. However, the STM response to the CDW modulation shows an anomalously large enhancement of the z deflection similar to that observed in $1T\text{-TaS}_2$. This provides indirect evidence that the major FS reconstruction and the magnitude of the associated charge transfer are similar in the CDW phases of the two compounds. The CDW modulations dominate the STM profiles in both materials and the atomic modulation shows a weak contribution to the z deflection. However, the atomic modulation in $1T\text{-TaSe}_2$ is systematically weaker than observed in the STM scans of $1T\text{-TaS}_2$ and in some cases is completely absent. This subtle difference in STM response is hard to quantify, but may reside in the detailed electronic structure of both the condensed CDW electrons and the remaining normal electrons. In $1T\text{-TaSe}_2$ evidence from nuclear quadrupole interaction studies²⁰ suggests that the central Ta atom has a maximum in electron density while the 12 remaining atoms of the 13-atom cluster show a slight electron deficiency. The same experiments on $1T\text{-TaS}_2$ show the central Ta atoms and its six nearest neighbors to have a nearly uniform charge density in agreement with the calculations of Smith *et al.*¹⁸ This difference could certainly influence the details of the STM profiles and additional high-sensitivity profile studies are planned. Mechanisms

for enhancing the STM response and their dependence on the detailed topology of the reconstructed FS will be discussed in Sec. IV B.

The major difference in low-temperature conductivities between $1T\text{-TaSe}_2$ and $1T\text{-TaS}_2$ has a clear impact on the STM scans at 4.2 K. The STM images of $1T\text{-TaSe}_2$ are very similar at both 77 and 4.2 K and the profiles of z deflection show the same relative variations between CDW and atomic modulation amplitudes. The z deflection associated with the CDW is $\geq 2 \text{ \AA}$ at both temperatures. In contrast, STM scans on $1T\text{-TaS}_2$ at 4.2 K with high-quality atomic resolution are difficult to obtain. The presence of the incipient metal insulator transition at 4.2 K and the low conductivity causes substantial instability in the tunneling characteristic and although the CDW superlattice can be resolved, no images with sufficient atomic resolution for satisfactory comparison to the $1T\text{-TaSe}_2$ data have been obtained. The I versus V and dI/dV versus V characteristics at 4.2 K show consistent structure indicating a CDW gap of $\sim 150 \text{ mV}$ in both $1T\text{-TaS}_2$ and $1T\text{-TaSe}_2$. However, the I versus V curves in $1T\text{-TaS}_2$ at 4.2 K show substantial variations in slope at bias voltages above and below the gap suggesting variations in the effective tunneling barrier from run to run, which are not observed at 77 K.

3. $1T\text{-VSe}_2$

$1T\text{-VSe}_2$ is a good d -band metal with a resistivity of $\sim 10^{-4} \Omega \text{ cm}$ at room temperature. The structure has one octahedral coordination layer per unit cell and trigonal symmetry with lattice constants $a_0 = 3.35 \text{ \AA}$ and $c_0 = 6.10 \text{ \AA}$ at room temperature. It has an unusually high value (1.82) of the c_0/a_0 ratio and the CDW superlattice is quite different from those observed in $1T\text{-TaSe}_2$ and $1T\text{-TaS}_2$. Diffraction studies by a number of authors (Williams,²¹ Tsutsumi *et al.*,²² van Landuyt *et al.*,²³ and Fung *et al.*²⁴) have suggested a variety of superlattice formations during cooling of the crystals. Williams²¹ reported an incommensurate superlattice at 140 K and a commensurate $4a_0 \times 4a_0 \times 3c_0$ superlattice at 40 K. van Landuyt *et al.*³³ analyzed diffraction data obtained as the crystal was cooled on a microscope stage from room temperature to liquid-nitrogen temperature. They detected at least three separate \mathbf{q} vectors forming during cool down and concluded that at least three separate phase transitions occurred. One of these was identified as a superlattice with a wavelength equal to $\sqrt{7}a_0$ while analysis of the complex electron diffraction patterns also identified several other possible \mathbf{q} vectors and wavelengths.

At 77 K and below we see no evidence of these higher-temperature phases and detect only the $4a_0 \times 4a_0 \times 3c_0$ superlattice as confirmed by recent electron and x-ray diffraction studies. Studies by Tsutsumi,⁴ Yoshida and Motizuki,²⁵ and Eaglesham *et al.*¹³ generally agree on a CDW superlattice at low temperature which is commensurate within the layer with a wavelength component of $4a_0$ and incommensurate perpendicular to the layers with a wavelength component of $\sim 3c_0$. Tsutsumi⁴ reports an abrupt change in the component along c at 85 K, but is in agreement with previous results on the low-

temperature \mathbf{q} vector. His measured value of the \mathbf{q} vector below 85 K is $\mathbf{q}=0.250\mathbf{a}^*+0.307\mathbf{c}^*$.

Although $1T\text{-TaSe}_2$ and $1T\text{-VSe}_2$ have similar high-temperature FS's there is a significant difference between the Ta and V compounds. The d -based band in $1T\text{-TaSe}_2$ is separated by a large gap (~ 0.1 Ry) from the chalcogen p -based valence band, while in the more covalently bonded $1T\text{-VSe}_2$ the d -based band shows significant overlap with the p band. The strong p/d hybridization is expected to give rise to a more complicated pattern of FS-driven instabilities than occurs in the Ta-based compounds. In addition to nesting of the electron and hole sheets inside the d -based bands with wave vectors parallel to the ΓM directions, nesting of the electron-hole surfaces can occur between the d -based conduction band and the p -based valence band.

These differences in the band-structure details lead to a major difference in the CDW formation. In contrast to $1T\text{-TaSe}_2$, the \mathbf{q} vectors in the metal plane of $1T\text{-VSe}_2$ are equal to $a^*/4$ rather than $a^*/\sqrt{13}$, thereby changing the low-temperature BZ and generating a completely different band folding geometry for determination of the low-temperature FS.

The STM deflection profiles in $1T\text{-VSe}_2$ are dominated by the atomic modulation in contrast to $1T\text{-TaSe}_2$ where the CDW modulation generates the dominant STM deflection. This suggests a much weaker modification in the LDOS generated by the CDW formation in $1T\text{-VSe}_2$, consistent with a major difference in band folding, FS obliteration, and $2k_F$ mixing. No calculations are presently available of the band structure in the CDW phase, but the STM results suggest a FS and CDW structure more characteristic of the trigonal prismatic phases, a conclusion consistent with the differences in band structure and FS reconstruction that exist between $1T\text{-VSe}_2$ and $1T\text{-TaSe}_2$.

As pointed out in the experimental results, the STM scans at both 77 and 4.2 K show strong evidence of broken symmetry in the expected triple- \mathbf{q} CDW structure. Many of the STM scans are dominated by a CDW superlattice characteristic of a double- \mathbf{q} structure with the third component either absent or very weak. Evidence of a triple- to double- \mathbf{q} transition below ~ 80 K has also been obtained from electron diffraction experiments carried out by Eaglesham *et al.*¹³ On cooling below ~ 110 K they observed the development of satellite reflections which could be indexed as $\mathbf{g}+\mathbf{q}_j$ where \mathbf{g} is a reciprocal sublattice vector and $\mathbf{q}_1=(0.25a^*, 0, 0.314c^*)$, $\mathbf{q}_2=(0, 0.25b^*, 0.314c^*)$, and $\mathbf{q}_3=(-0.25a^*, -0.25b^*, 0.314c^*)$. These three \mathbf{q}_j are parallel to the three mirror planes of the basic crystal structure generally consistent with the triple- \mathbf{q} CDW symmetries seen in the other layer compounds.

When the crystal was subsequently cooled below 80 K, the diffraction pattern was observed to undergo a sudden change. The q_z component was shifted to $0.307c^*$ and a broken symmetry developed in which only two of the three \mathbf{q}_j variants were present. The crystal was also observed to develop a well-defined domain structure which, when imaged using the three types of satellites ($\mathbf{q}_1, \mathbf{q}_2, \mathbf{q}_3$),

showed two bright images and one dark image for each separate domain.

The presence of these domains exhibiting a double- \mathbf{q} structure can easily explain the STM results which scan an area within only one domain. Different runs with the tunneling tip sampling different domains show substantial variations in the double- \mathbf{q} versus triple- \mathbf{q} structure. A STM study of a single domain as a function of temperature above 80 K would be important for clarifying the STM response.

B. CDW amplitudes in STM scans

The CDW superlattices in $1T\text{-TaS}_2$ and $1T\text{-TaSe}_2$ produce STM z deflections up to 5 Å and indicate an unusually large response to the FS rearrangement induced by the CDW. Tersoff²⁶ has suggested a mechanism for enhancement of the STM response which applies specifically to semiconductors and semimetals of low effective dimensionality. Whenever the FS collapses to a point at the corner of the surface Brillouin zone, the STM image will in effect correspond to an individual state. This state will have a nodal structure and the STM will respond to this nodal structure which has the periodicity of the unit cell involved in the FS collapse.

The Tersoff²⁶ analysis was originally developed for graphite where the FS of a single layer collapses to a point at the corner of the projected two-dimensional BZ. The CDW's considered here represent a quasi-two-dimensional (2D) structure and generate a hexagonal structure with three equivalent \mathbf{q} vectors at relative orientations of 120° . The associated wave functions can be expanded as six plane waves and, if the band edge falls near the BZ corners, the model will generate a hexagonal array of singular dips. In the case of the quasi-2D layer structures the FS collapse will not be complete and the nodal structure will depend on the degree of FS obliteration and the strength of mixing between \mathbf{k}_\parallel and $\mathbf{k}_\parallel+\mathbf{G}$ wave functions. Tersoff²⁷ has calculated the nodal structure for various cases of FS collapse and mixing and four examples are shown in Fig. 23. Figure 23(a) shows contours of constant LDOS for total FS elimination and strong mixing by a CDW of wavelength $5a_0$. The nodal structure is extremely strong in this case. For only partial FS elimination the nodal structure is weaker, but is still quite large when the mixing is strong as shown in Fig. 23(b). With only partial elimination of the FS and weaker mixing, the nodal structure is substantially reduced but still evident as shown in Fig. 23(c) while very weak mixing gives a pattern dominated by the atomic modulation as shown in Fig. 23(d). The relative amplitudes of the nodal structure and the atomic modulation are essentially determined by the degree of \mathbf{k}_\parallel and $\mathbf{k}_\parallel+\mathbf{G}$ mixing and FS obliteration. The profiles generated by the above model can clearly be adjusted to fit the whole range of experimental profiles measured for the wide variety of CDW amplitudes observed in the layer-structure dichalcogenides.

Elastic deformation of the tunneling tip or the sample surface during close approach of the tip to the surface could also be playing a role. This mechanism of surface

deformation was suggested by Soler *et al.*²⁸ as a possible explanation of the giant corrugations observed in STM scans of graphite. However, deformation of the tip may require less energy in most cases. If the tip-surface distance decreases below a few angstroms the atomic forces become repulsive and can induce some degree of deformation in either the tip or the surface. This would be detected as an additional change in effective z deflection and would be modulated at the atomic wavelength and produce an overall enhancement of the intrinsic structure observed in the STM scan. This amplification would decrease rapidly as the tunneling distance is increased. The effective barrier height measurement given in Sec. III F is consistent with such a mechanism particularly in the case of $1T$ -VSe₂. The deformation would decrease as the tunnel distance increases with bias voltage and this would increase dI/dz leading to an apparent increase in effective barrier height as observed in Figs. 22(a) and 22(b).

The relative importance of the two mechanisms outlined above in contributing to the anomalous z deflection is difficult to quantify. However, comparison of the results on $1T$ -TaSe₂ and $1T$ -TaS₂ to those on $1T$ -VSe₂ sug-

gests that a significant difference exists in the magnitude of the effective barrier height and its dependence on tunneling distance (see Fig. 22). The main difference between these two tunneling experiments is the electronic and CDW structure of the substrate, since the tunneling tip is the same in both experiments. One concludes that in the presence of a strong CDW, as in $1T$ -TaSe₂, the effective barrier height increases much more slowly than in $1T$ -VSe₂ consistent with a large contribution from electronic structural effects such as in the model of Tersoff.^{26,27} The very rapid and somewhat variable changes in effective barrier height observed for $1T$ -VSe₂ could be interpreted as a deformation effect which would be very sensitive to the precise tunneling distance. The deformation effects could be associated with either the tip, the substrate, or intermediate elements such as adsorbed molecules or oxides. Further detailed studies will be needed to quantify the possible contributions, but the data suggest that more than one mechanism is operating and that electronic structural differences associated with different CDW formation play an important role in the large corrugation that is observed.

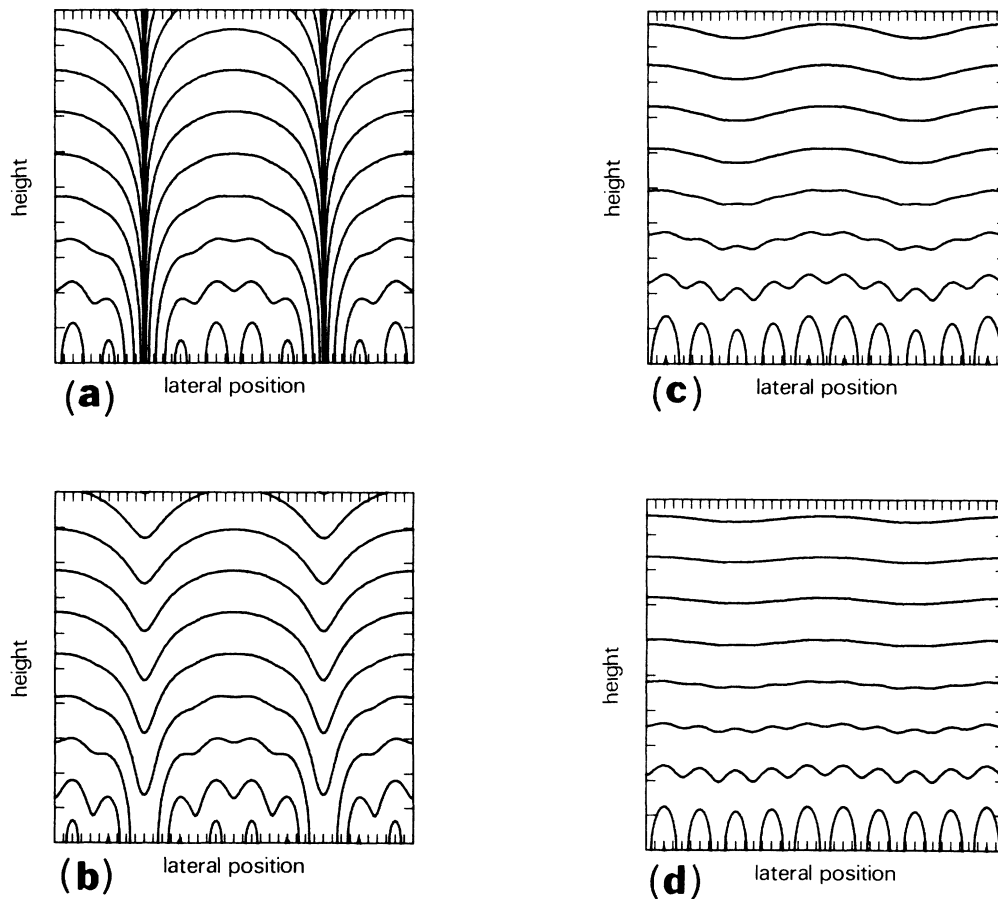


FIG. 23. Contours of constant LDOS calculated for various degrees of FS collapse and mixing of wave functions at \mathbf{k}_{\parallel} and $\mathbf{k}_{\parallel} + \mathbf{G}$. They show the relative amplitudes of superimposed atomic and CDW modulation in four cases for a CDW wavelength of $5a_0$. (a) Total FS elimination and strong mixing. (b) Partial FS elimination and strong mixing. (c) Partial FS elimination and weak mixing. (d) Partial FS elimination and very weak mixing (Ref. 27, Tersoff, unpublished).

C. High-temperature CDW structure in $1T\text{-TaS}_2$ and $1T\text{-TaSe}_2$

The majority of the experiments discussed in this report were performed at 77 and 4.2 K and therefore measure the properties of the commensurate CDW phase of $1T\text{-TaS}_2$ and $1T\text{-TaSe}_2$. In order to check the response of our STM's at higher temperatures we have also made room-temperature scans on both materials using the same batches of crystals as used for the low-temperature experiments.

The CDW in $1T\text{-TaSe}_2$ remains commensurate up to room temperature and above, while in $1T\text{-TaS}_2$ the CDW undergoes a commensurate to incommensurate transition as the temperature is increased above 120–150 K and several subphases of the incommensurate CDW state have been observed.^{5,29} The room-temperature STM scans of $1T\text{-TaSe}_2$ have indicated a uniform CDW amplitude to exist over the maximum single scan areas of $\sim 250 \times 250 \text{ \AA}^2$ that are covered by our STM's. The patterns of CDW maxima show a uniform hexagonal pattern indistinguishable from that observed for $1T\text{-TaSe}_2$ at 77 and 4.2 K. The CDW amplitude is also completely dominant compared to the atomic amplitude. Total z deflections of 3–5 Å are observed which are as large as or larger than those observed at low temperatures.

In the case of $1T\text{-TaS}_2$ at room temperature the pattern of CDW maxima clearly reflects the presence of an incommensurate CDW in that the patterns of CDW maxima show variations over intervals of approximately six CDW wavelengths ($\sim 76 \text{ \AA}$). At room temperature the average angle between the CDW superlattice and the atomic lattice is $\sim 12^\circ$ compared to the low-temperature commensurate angle of 13.9° . As was the case at low temperature the STM scans show varying degrees of atomic resolution but the z deflection continues to be dominated by the CDW modulation amplitude.

In STM scans where the CDW modulation is completely dominant we detect a weak continuous modulation of the CDW amplitude with a period of approximately six CDW wavelengths. This gives rise to a modulated two-dimensional structure where the CDW shows maximum amplitude at the center region and minimum amplitude at the edges. A gray-scale scan of such a structure is shown in Fig. 24(a) and an enhanced picture using a color look up table (LUT) for contrast is shown in Fig. 24(b).

A profile spanning approximately two of the long-range modulation periods is shown in Fig. 25. This profile was recorded along the long trace in Fig. 24(a) and clearly shows a continuous modulation of the CDW amplitude. Both the CDW maxima and minima are modulated as would be characteristic of an absolute modulation of the CDW amplitude. The atomic modulation in this scan is a negligible fraction of the maximum z deflection of $\sim 4 \text{ \AA}$ and is only a small fraction of the long-range modulation of the CDW amplitude which is $\sim 2 \text{ \AA}$.

Three profiles recorded along traces intersecting at the center of one of the two-dimensional modulation zones are shown in Fig. 26. The corresponding traces are indicated in Fig. 24(a) and are oriented at 120° angles. These

profiles demonstrate that the maximum CDW amplitude occurs at the center of the two-dimensional regions of CDW amplitude modulation. The amplitude continuously decreases out to the boundary regions.

In STM scans of $1T\text{-TaS}_2$ at room temperature where the superimposed atomic structure is resolved the long-range modulation of the CDW amplitude also produces a two-dimensional pattern which has an average repeat distance of about six CDW wavelengths. The presence of the superimposed CDW and atomic modulations make determination of the absolute CDW amplitude more difficult. The atom intensity pattern surrounding each CDW maximum shows the characteristic intensity variation due to the presence of the CDW amplitude arising from the Ta-atom layer below the surface S atoms as shown in the STM scan of Fig. 27. These atom intensity patterns near CDW maxima vary considerably and do not show any large two-dimensional regions in which the local atomic intensity patterns around the CDW maxima

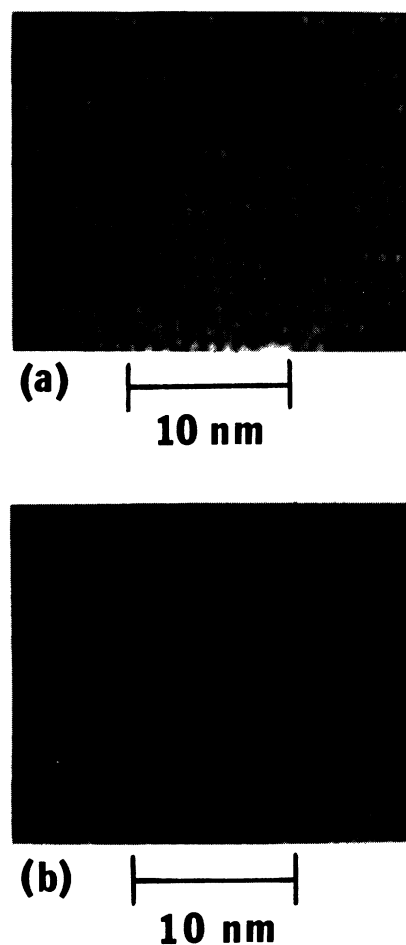


FIG. 24. (a) Gray-scale STM image of $1T\text{-TaS}_2$ at room temperature showing a two-dimensional modulated structure of CDW maxima. The surface S atoms are not resolved in this scan. (b) Higher contrast image of scan in (a) obtained by using a color LUT. Two-dimensional regions are created by long-range modulation of the CDW amplitude. ($I = 2.2 \text{ nA}$, $V = 25 \text{ mV}$.)

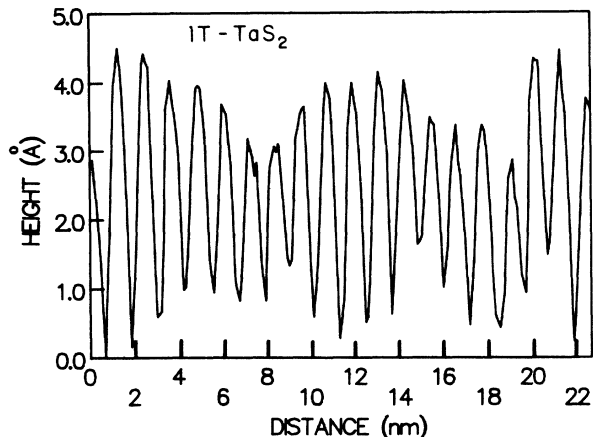


FIG. 25. Profile of the z deflection observed along the long track in Fig. 24(a). The track spans approximately two periods of the long-range CDW amplitude modulation. Each period corresponds to about six CDW wavelengths and a continuous modulation of the CDW amplitude is observed. The modulation amplitude is $\approx 2 \text{ \AA}$.

are identical as observed in the low-temperature commensurate phase.

We detect an overall two-dimensional modulation structure with boundaries where the CDW amplitudes reach a minimum. These are generally consistent with the long-range modulation period of about six CDW wavelengths. The boundary regions show irregularities in the superimposed atom and CDW amplitudes that are equivalent to a phase shift of approximately one atomic spacing in the position of the CDW maxima relative to the positions of the surface sulfur atoms. We have examined the profiles of modulation along tracks running at the average CDW direction of $\sim 12^\circ$ to the atomic lattice and also along segments of tracks running at the commensurate angle of 13.9° with a shift of one atom spacing in the boundary region. The two types of profile are shown in Figs. 28 and 29 and are recorded along the tracks indicated in Fig. 27. In Fig. 28 the profile is recorded along tracks oriented at 13.9° to the lattice and a phase shift of one atomic spacing has been introduced at the position of the arrow. The corresponding tracks with the phase shift are indicated in Fig. 27 as identified by the 13.9° angle. The profiles in Fig. 29 are recorded along tracks running at the average CDW angle of $\sim 12^\circ$. These represent two close tracks displaced from each other by $\sim a_0/2$ but running through the same row of CDW maxima. These tracks are also indicated in Fig. 27 and are labeled with the 12° angle.

Within the accuracy of the STM response all of these profiles show a variation in amplitude that corresponds to a modulation period of about six CDW wavelengths. The presence of the atoms generates superimposed peaks of up to $\sim 0.5 \text{ \AA}$ which complicate the evaluation of the CDW amplitude modulation. However, all of the profiles are consistent with the absolute CDW modulation observed in Figs. 24–26 where the atom modulation is

negligible. So far we have observed no large regions of uniformly enhanced atomic clusters with constant amplitude that would indicate a region of commensurate CDW's.

At present our data are consistent with a gradual modulation of the CDW amplitude resulting from an incommensurate CDW giving a slightly different charge transfer and LDOS modification in each 13-atom cluster

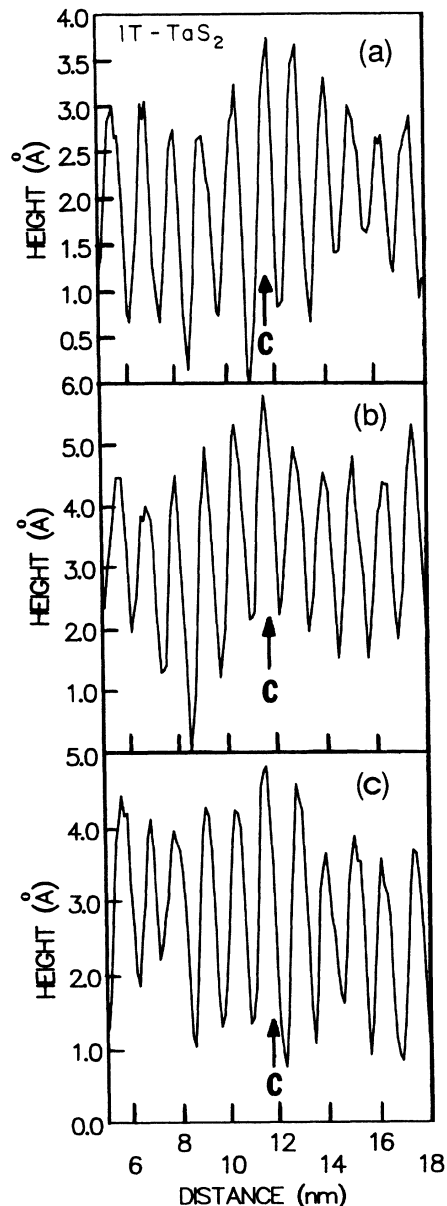


FIG. 26. Profiles of z deflection observed along three short tracks intersecting at the center of one of the two-dimensional regions. The tracks are shown in Fig. 24(a) and the center CDW maximum is marked by C in the profiles. The tracks are oriented at 120° intervals and show that the CDW amplitude decreases approximately uniformly from the center maximum out to the boundaries.

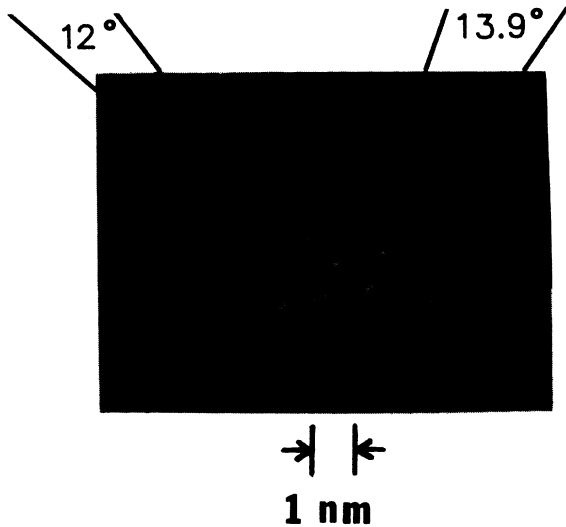


FIG. 27. Gray-scale image of $1T\text{-TaS}_2$ at room temperature showing both atom and CDW modulation. Long-range modulation of the CDW maxima is also present. The atomic intensity pattern near each CDW maximum shows continuous variation. No extended regions of CDW maxima showing the same atomic intensity pattern are observed indicating the absence of commensurate CDW regions. ($I=2$ nA, $V=6$ mV.)

associated with a CDW maximum. The long-range modulation of CDW amplitude will repeat at regular intervals as determined by the phase accumulation between the CDW and atomic lattices. This will generate two-dimensional regions of CDW maxima separated by boundaries where the CDW amplitude reaches a minimum and the accumulated phase shift is equivalent to one atomic spacing. For the average room-temperature angle of $\sim 12^\circ$ between the atomic and CDW lattices the ob-

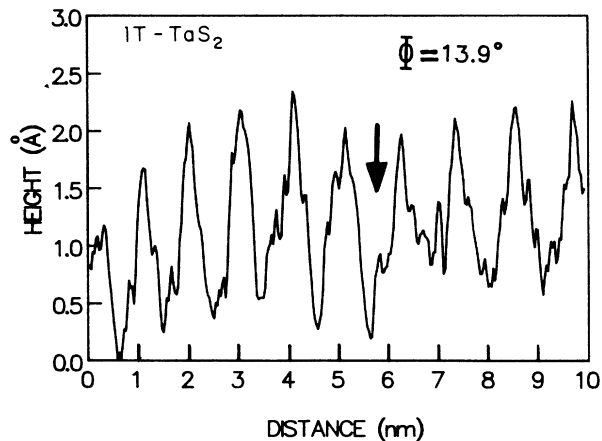


FIG. 28. Profile of z deflection observed along the tracks shown on the right of Fig. 27 and oriented at the commensurate angle of 13.9° relative to the atom rows as indicated in Fig. 27. The profile comprises two sections displaced laterally by one atomic spacing at the position of the arrow. Long-range modulation of the CDW amplitude is still observed.

served repeat distance of about six CDW wavelengths is consistent with the incommensurate structure expected. Near the center of the modulation region where the CDW amplitude is maximum the CDW will be at the most favorable phase position for lock-in to the lattice. Whether the q vector changes in response to this or remains uniform cannot be detected in these experiments. The continuous change of CDW amplitude suggests that if lock-in occurs it does not extend over a significant number of CDW wavelengths.

There has been considerable discussion³⁰ and analysis of diffraction data in regard to the possible existence at room temperature of commensurate domains separated by discommensurations. Nakanishi and Shiba³¹ and Nakanishi *et al.*³² have predicted a domainlike CDW state with 13 hexagonal domains surrounded by narrow discommensurations based on theoretical models. Yamamoto³³ has argued that analysis of the higher-order satellite reflections observed in x-ray diffraction data on

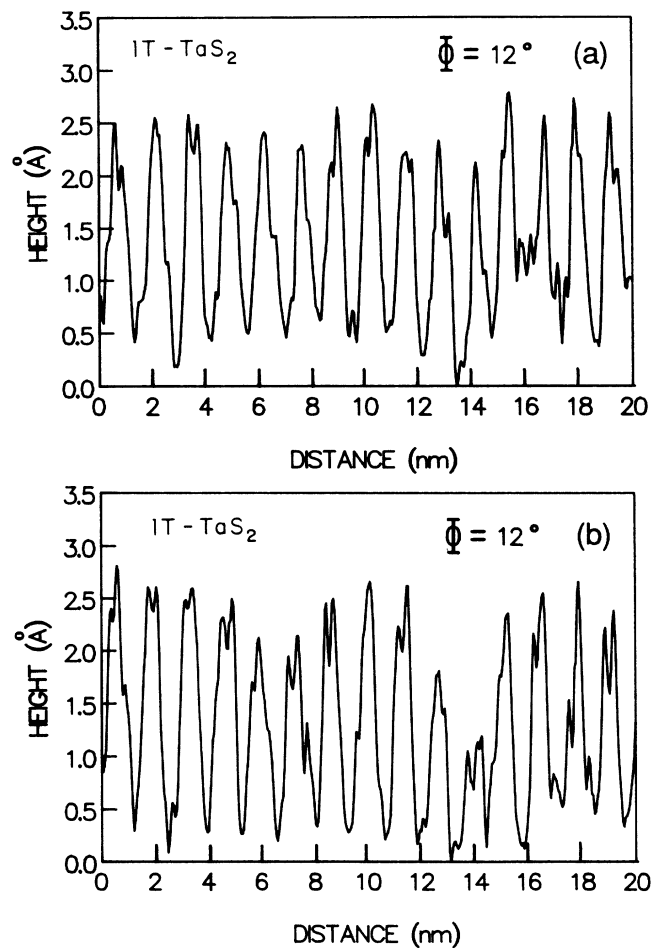


FIG. 29. Profiles of z deflection along the tracks running to the left-hand side of Fig. 27 and oriented at an angle of $\sim 12^\circ$ to the atom rows. The profiles in (a) and in (b) are laterally separated by $a_0/2$. Both show a long-range CDW amplitude modulation of about six CDW wavelengths.

1T-TaS₂ at room temperature gives results consistent with the diffraction expected from such a domain structure.

Our STM data do not detect sharp discommensuration boundaries. If discommensurations exist they are quite diffuse and do not induce abrupt changes in CDW amplitude. The observed changes in CDW amplitude occur over a number of CDW wavelengths indicating that the changes in charge transfer, LDOS, and periodic lattice distortion induce a continuous amplitude modulation of the CDW. At present the STM data are not sufficiently accurate to detect the precise spatial variation in CDW amplitude and profile, but we do not detect any clear evidence of commensurate domains.

Wu and Lieber³⁴ have reported a similar two-dimensional structure in 1T-TaS₂ observed with a STM at room temperature. They have analyzed the structure in terms of two-dimensional domains where the CDW is commensurate separated by boundaries where the CDW amplitude decreases and phase slip occurs. They support this argument with estimates of the local angles between the atomic and CDW lattices. They suggest that the CDW amplitudes change rather abruptly at the domain boundaries and that the phase slips in the CDW lattice are localized. At present our data do not confirm this analysis and are more consistent with a gradual change in CDW amplitude. Considerably more STM data on 1T-TaS₂ will be required in order to clearly resolve this issue.

V. CONCLUSIONS

Continued STM studies of 1T-TaSe₂ and 1T-TaS₂ at 300, 77, and 4.2 K have shown that both the atomic and CDW modulations can be simultaneously resolved. Studies⁵ at intermediate temperatures can also resolve atoms fairly well, but careful measurements of relative amplitudes have not yet been made. The amplitude of the atomic modulation at 77 K and below remains small relative to the anomalously large CDW amplitude, but shows a wide variation in resolution for different runs at both 77 and 4.2 K. The contours of constant LDOS, which are dominated by the $\sqrt{13}\mathbf{a}_0 \times \sqrt{13}\mathbf{a}_0$ superlattice, sometimes show strong perturbations by the atomic potential, while in other runs little or no perturbation by the atomic potential is observed. The STM modulation at the CDW wavelength remains ≥ 2 Å and results indicate that the FS modifications by the CDW are a major contributing factor to the STM corrugation. This conclusion is supported in part by a comparison of the CDW modulations observed in 1T-TaSe₂ and 1T-TaS₂ to that observed in 1T-VSe₂, where the relative CDW to atomic modulation is much smaller, consistent with a weak CDW and a significantly reduced FS obliteration in 1T-VSe₂. The correlation of the z deflection at the CDW wavelength with the electronic structure is most likely a result of singularities in the LDOS produced by the CDW. The strength of these singularities in the LDOS is related to obliteration of the FS by the CDW and the associated mixing of states at $2k_F$. A model calculation of these singularities has been given by Tersoff^{26,27} and can easily

be adjusted to fit the data.

At room temperature the STM scans on 1T-TaS₂ show the clear presence of the incommensurate CDW while the STM scans on 1T-TaSe₂ show a commensurate CDW structure as expected. In 1T-TaS₂ a long-range modulation of the CDW amplitude gives rise to a two-dimensional modulated structure. The CDW amplitude is maximum at the center of each region and decreases by ~ 1 Å at the edges. The diameter of these regions is about six CDW wavelengths. This long-range continuous amplitude modulation appears consistent with a continuously incommensurate CDW. So far we have not observed definite evidence of any commensurate regions of significant size at room temperature.

The anomalously large and somewhat variable amplitude produced by the CDW modulation can also have other contributing factors in addition to the LDOS singularities. Deformation of the tip or the surface due to the atomic hard core repulsive potential may play a role in the enhanced z deflection observed in the STM images of the 1T compounds. There is also evidence from the low-temperature conductance (dI/dV) versus voltage curves that impurities or defects at the tip or on the surface can enhance the total z deflection. The presence of large zero-bias anomalies has been observed at 4.2 K and these correlate with large z deflections and lowered barrier heights. Additional details of the zero-bias anomalies have been discussed by Wang *et al.*³⁵ An analysis of the effective barrier height as a function of tunneling distance indicates that the deformation mechanism, if important, plays a greater role in the STM scans of 1T-VSe₂ than in the scans of 1T-TaSe₂ and 1T-TaS₂ where the CDW structure dominates.

In contrast to the STM results on the 1T phases of TaS₂ and TaSe₂, and STM scans of 1T-VSe₂ confirm the presence of a CDW modulation due to a $4\mathbf{a}_0 \times 4\mathbf{a}_0$ superlattice that generates a completely different STM response. In 1T-VSe₂ the CDW modulation is not dominant relative to the atomic modulation and the triple- q symmetry of the CDW superlattice pattern is broken. At 4.2 K evidence of a triple- to double- q transition is observed and a variable domain structure is suggested by major variations in the CDW pattern detected by the STM. These results are consistent with the calculated differences in the band structure and FS and with the recent observations in electron diffraction experiments.¹³ Free energy calculations indicate that the energy difference between the triple- q and double- q structure is relatively small.

The local CDW modulation in all three 1T-phase compounds can be strongly perturbed by localized defects. These defects are generally characterized by missing CDW maxima and a local modification of the STM profile within a few atomic wavelengths. The most likely causes are vacancies or impurities in the metal layer that interrupt the charge transfer induced by the CDW. Surface Se-atom vacancies may also play a role in 1T-VSe₂.

The STM studies on the 1T-phase crystals demonstrate the power of the STM to resolve both the atomic structure and the superimposed electronic structural modifications. Subtle differences in the CDW structure,

the relative CDW to atomic amplitudes, defects in the CDW structure, and domains of different CDW symmetry can all be detected with high sensitivity. The studies suggest that modifications due to doping with impurities, intercalation, or temperature variation can be detected with the STM and should provide excellent comparisons to the pure phase results demonstrated here. Some comparison with results obtained operating in high vacuum and with ultraclean surface preparation conditions would also be interesting. The source of ZBA's and their role in

the observed z deflections could be clarified with such experiments.

ACKNOWLEDGMENTS

This research has been supported by the U.S. Department of Energy under Grant No. DE-FG05-84ER45072. The authors have benefitted from useful discussions with Vittorio Celli, Paul Hansma, Joe Demuth, and Andy Johnson. Barney Drake has contributed to the design and construction of the STM's.

-
- ¹J. A. Wilson, F. J. Di Salvo, and S. Mahajan, *Adv. Phys.* **24**, 117 (1975).
²A. M. Woolley and G. Wexler, *J. Phys. C* **10**, 2601 (1977).
³D. E. Moncton, F. J. Di Salvo, and S. C. Davey, *Bull. Am. Phys. Soc.* **24**, 446 (1979).
⁴K. Tsutsumi, *Phys. Rev. B* **26**, 5756 (1982).
⁵R. E. Thomson, U. Walter, E. Ganz, J. Clarke, A. Zettl, P. Rauch, and F. J. DiSalvo, *Phys. Rev. B* **38**, 10734 (1988).
⁶C. G. Slough, W. W. McNairy, R. V. Coleman, B. Drake, and P. K. Hansma, *Phys. Rev. B* **34**, 994 (1986).
⁷R. V. Coleman, B. Drake, B. Giambattista, A. Johnson, P. K. Hansma, W. W. McNairy, and G. Slough, *Phys. Scr.* **38**, 235 (1988).
⁸X. L. Wu, P. Zhou, and C. M. Lieber, *Phys. Rev. Lett.* **61**, 2604 (1988).
⁹F. J. DiSalvo, J. A. Wilson, B. G. Bagley, and J. V. Waszczak, *Phys. Rev. B* **12**, 2220 (1989).
¹⁰B. Drake, R. Sonnenfeld, J. Schneir, P. K. Hansma, G. Slough, and R. V. Coleman, *Rev. Sci. Instrum.* **55**, 441 (1986).
¹¹R. V. Coleman, B. Giambattista, P. K. Hansma, A. Johnson, W. W. McNairy, and C. G. Slough, *Adv. Phys.* **37**, 559 (1988).
¹²B. Giambattista, A. Johnson, R. V. Coleman, B. Drake, and P. K. Hansma, *Phys. Rev. B* **37**, 2741 (1988).
¹³D. J. Eaglesham, R. L. Withers, and D. M. Bird, *J. Phys. C* **19**, 359 (1986).
¹⁴J. Nogami, S. I. Park, and C. F. Quate, *Surf. Sci.* **203**, L631 (1988).
¹⁵S. Noutomi, T. Fatatsugi, M. Naito, and S. Tanaka, *Solid State Commun.* **50**, 181 (1984).
¹⁶L. F. Mattheiss, *Phys. Rev. B* **8**, 3719 (1973).
¹⁷H. W. Myron and A. J. Freeman, *Phys. Rev. B* **11**, 2735 (1975).
¹⁸N. V. Smith, S. D. Kevan, and F. J. Di Salvo, *J. Phys. C* **18**, 3175 (1985).
¹⁹N. J. Doran and A. M. Woolley, *J. Phys. C* **14**, 4257 (1981).
²⁰T. Butz (private communication).
²¹P. M. Williams, in *Crystallography and Crystal Chemistry of Materials with Layered Structure*, edited by F. Levy (Reidel, Dordrecht, 1976), p. 51.
²²K. Tsutsumi, T. Sambongi, T. Akira, and S. Tanaka, *J. Phys. Soc. Jpn.* **49**, 837 (1980).
²³J. van Landuyt, G. A. Wiegers, and S. Amelinckx, *Phys. Status Solidi* **46**, 479 (1978).
²⁴K. K. Fung, J. W. Steeds, and J. A. Eades, *Physica B+C (Amsterdam)* **99B**, 47 (1980).
²⁵Y. Yoshida and K. Motizuki, *J. Phys. Soc. Jpn.* **51**, 2107 (1984).
²⁶J. Tersoff, *Phys. Rev. Lett.* **57**, 440 (1986).
²⁷J. Tersoff (private communication).
²⁸J. M. Soler, A. M. Baro, N. Garcia, and H. Rohrer, *Phys. Rev. Lett.* **57**, 444 (1986).
²⁹S. Tanda, T. Sambongi, T. Tani, and S. Tanaka, *J. Phys. Soc. Jpn.* **53**, 476 (1984).
³⁰R. L. Withers and J. A. Wilson, *J. Phys. C* **19**, 4809 (1986).
³¹Kazuo Nakanishi and Hiroyuki Shiba, *J. Phys. Soc. Jpn.* **43**, 1839 (1977); **53**, 1103 (1984).
³²Kazuo Nakanishi, Hiroshi Takatera, Yasusada Yamada, and Hiroyuki Shiba, *J. Phys. Soc. Jpn.* **43**, 1509 (1977).
³³A. Yamamoto, *Phys. Rev. B* **27**, 7823 (1983).
³⁴Xian Liang Wu and Charles M. Lieber, *Science* **243**, 1703 (1989).
³⁵Chen Wang, B. Giambattista, C. G. Slough, and R. V. Coleman (unpublished).

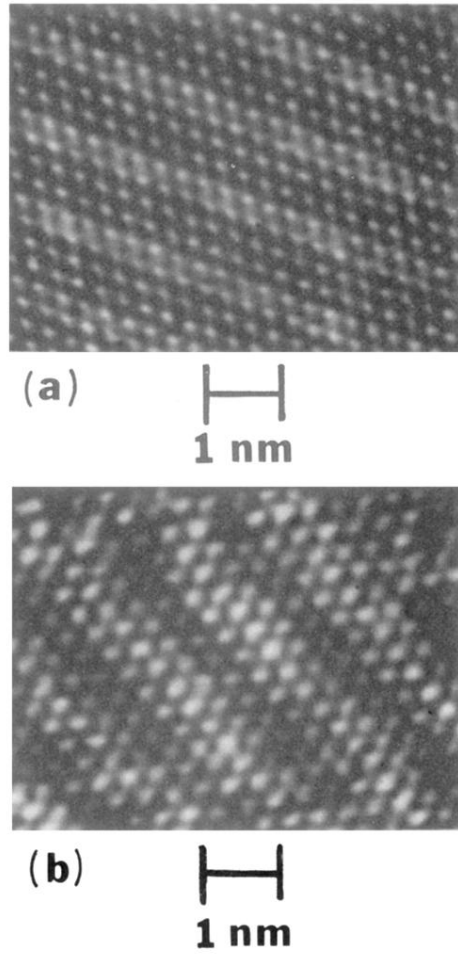
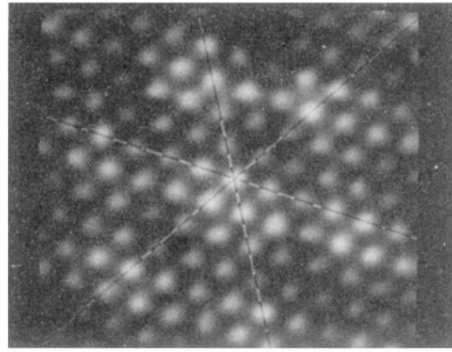
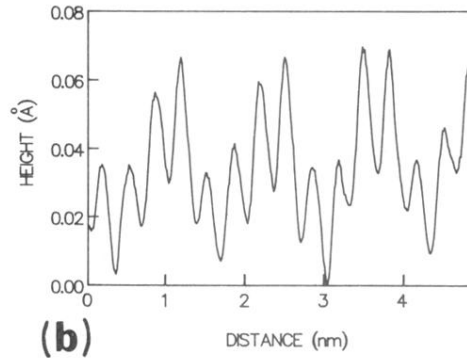


FIG. 10. Gray-scale images of STM scans on $1T\text{-VSe}_2$ showing unidirectional enhancement of the CDW pattern. (a) Scan at 4.2 K showing enhancement of two atomic rows along a single diagonal direction. ($I = 2.2$ nA, $V = 25$ mV.) (b) Scan at 77 K showing enhancement of three-atom rows along a single diagonal direction.

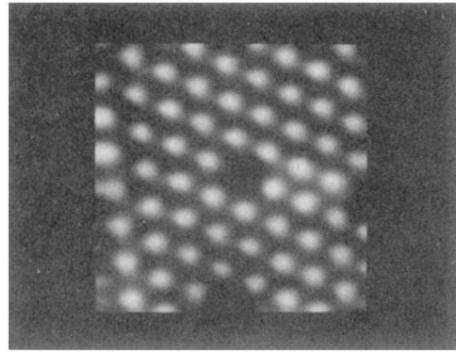


(a)  1 nm

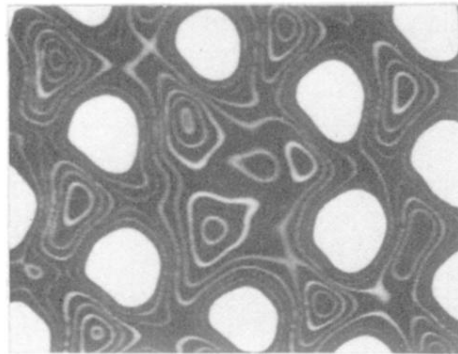


(b) DISTANCE (nm)

FIG. 11. (a) Gray-scale image of $1T\text{-VSe}_2$ at 4.2 K showing well-defined groups of seven surface Se atoms marking the positions of the CDW maxima. ($I=2.2$ nA, $V=25$ mV.) (b) Profile of the z deflection along one of the diagonal tracks in (a). All of the profiles show an extremely small modulation of ~ 0.07 Å which is dominated by the atomic modulation at a wavelength of $4a_0$.



(a) 
1 nm



(b) 
1 nm

FIG. 13. STM scans on $1T\text{-TaSe}_2$ at 4.2 K showing the presence of defects in the CDW superlattice. (a) Gray-scale image showing missing CDW maxima. Pattern is totally dominated by the CDW superlattice. (b) Contour plot of the STM scan shown in (a). Contours confirm the dominance of the CDW superlattice with the region of the missing CDW maximum showing a minimum and relatively uniform z deflection in the central region. From Ref. 11.

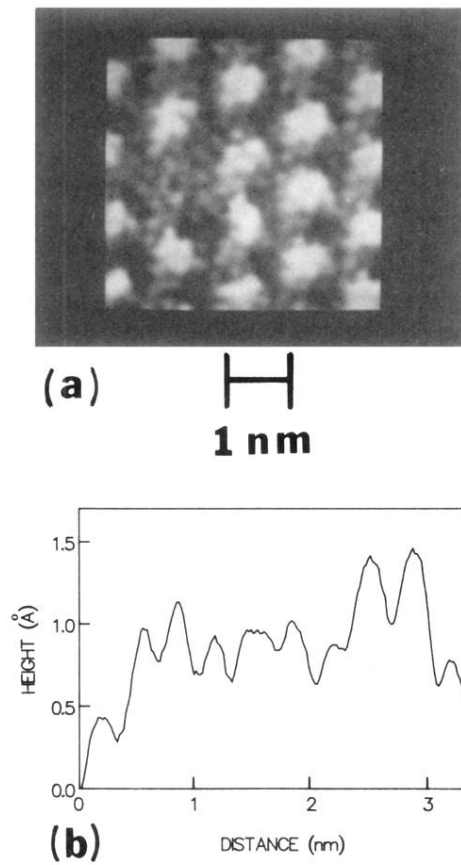


FIG. 14. (a) Gray-scale image of a STM scan on $1T\text{-TaS}_2$ at 77 K showing a missing CDW maximum. In this case the surface S atoms are resolved within the region of the missing maximum. (b) Profile of the z deflection across the center of the defect region shows a continuous modulation at the atomic wavelength. The defect does not appear to involve surface S atoms. ($I=2.2$ nA, $V=25$ mV.)

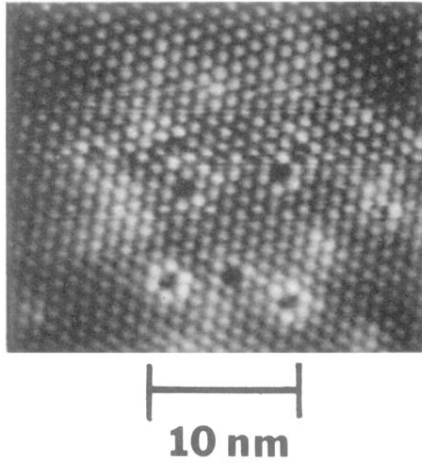
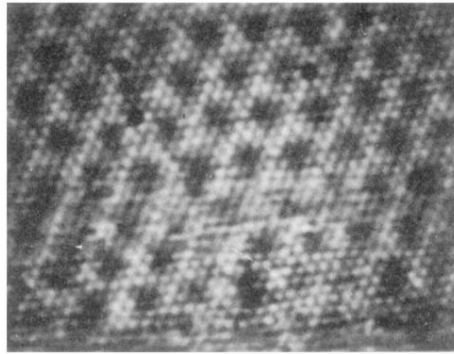
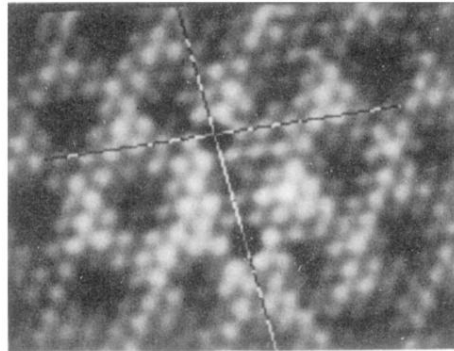


FIG. 15. Gray-scale image of a STM scan on $1T\text{-TaS}_2$ at 153 K. A number of defects involving missing CDW maxima are observed. Several of these involve enhancement of the surrounding CDW maxima while others do not show this enhancement. ($I=3$ nA, $V=47$ mV.)



(a) 
1 nm



(b) 
1 nm

FIG. 17. Gray-scale images of STM scans on $1T\text{-VSe}_2$ at 4.2 K showing defects in the pattern of surface Se atoms. The defects in this case are associated with missing surface Se atoms and do not have a specific correlation with the CDW superlattice. (a) Large area scan showing a number of distributed defects. Three defects in the upper half of scan are marked by localized black holes. (b) Magnified scan of two close defects near the CDW maxima. ($I = 2.2$ nA, $V = 25$ mV.)

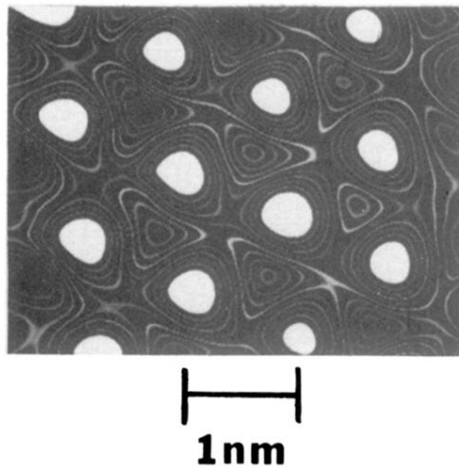
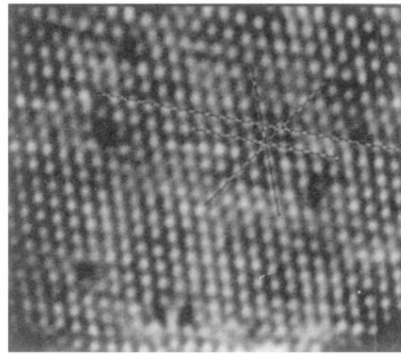
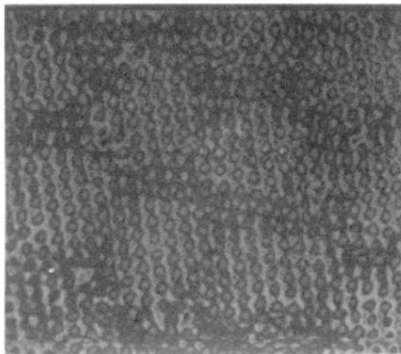


FIG. 2. STM scan at 4.2 K from the surface of a $1T$ -TaSe₂ crystal presented as contours of constant z deflection (constant LDOS). The contours in this STM scan detect only the CDW superlattice. ($I=2.2$ nA, $V=30$ mV.)



(a) 
10 nm



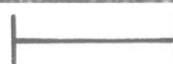
(b) 
10 nm

FIG. 24. (a) Gray-scale STM image of 1T-TaS₂ at room temperature showing a two-dimensional modulated structure of CDW maxima. The surface S atoms are not resolved in this scan. (b) Higher contrast image of scan in (a) obtained by using a color LUT. Two-dimensional regions are created by long-range modulation of the CDW amplitude. ($I=2.2$ nA, $V=25$ mV.)

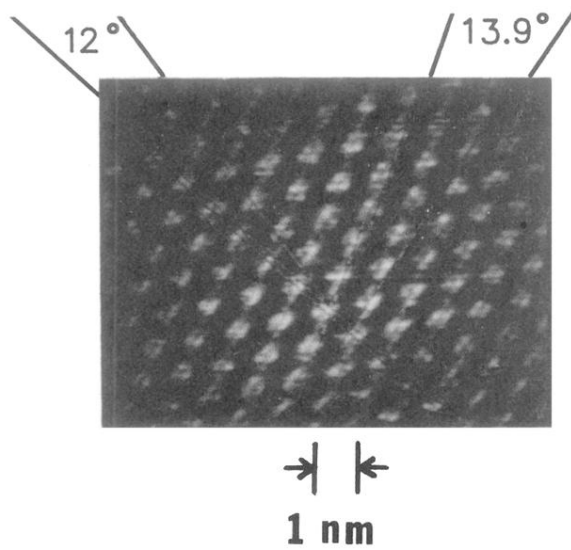
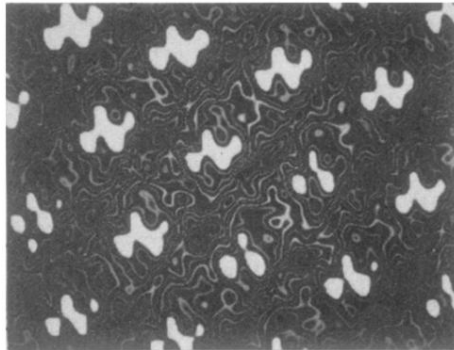
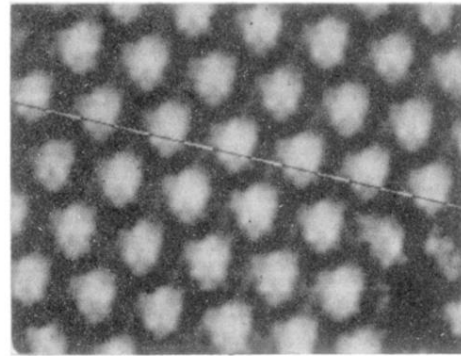


FIG. 27. Gray-scale image of $1T\text{-TaS}_2$ at room temperature showing both atom and CDW modulation. Long-range modulation of the CDW maxima is also present. The atomic intensity pattern near each CDW maximum shows continuous variation. No extended regions of CDW maxima showing the same atomic intensity pattern are observed indicating the absence of commensurate CDW regions. ($I=2$ nA, $V=6$ mV.)

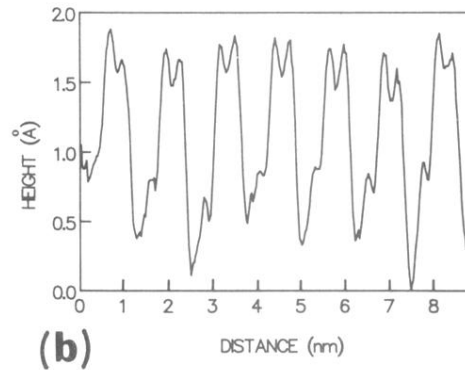


1 nm

FIG. 3. STM scan at 4.2 K from the surface of a $1T\text{-TaSe}_2$ crystal. Contours of constant z deflection in this case show a significant perturbation by the atomic modulation although the CDW superlattice is still dominant. ($I=2.2$ nA, $V=5$ mV.)

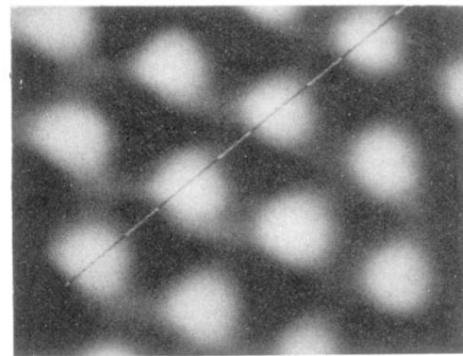


(a)  1 nm

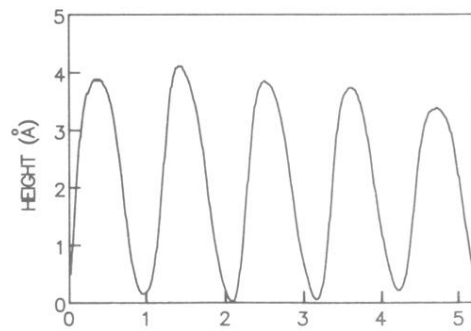


(b)

FIG. 4. (a) Gray-scale image of a STM scan on $1T\text{-TaSe}_2$ at 4.2 K. The surface Se atoms are resolved and appear as a superposition with the CDW modulation of much larger amplitude. White areas with a weak superimposed atomic modulation are centered on the CDW maxima which are displaced by $a_0/\sqrt{3}$ from the surface Se-atom positions. (b) Profile of the z deflection recorded along the track indicated in (a). The z deflection is dominated by the CDW with a very small atomic modulation.



(a) 
1 nm



(b) DISTANCE (nm)

FIG. 5. (a) Gray-scale image of a STM scan on $1T\text{-TaSe}_2$ at 4.2 K which detects only the CDW superlattice. (b) The profile along the track shown in (a) shows a very strong CDW deflection of $\sim 4 \text{ \AA}$, but shows no structure due to the atomic modulation.

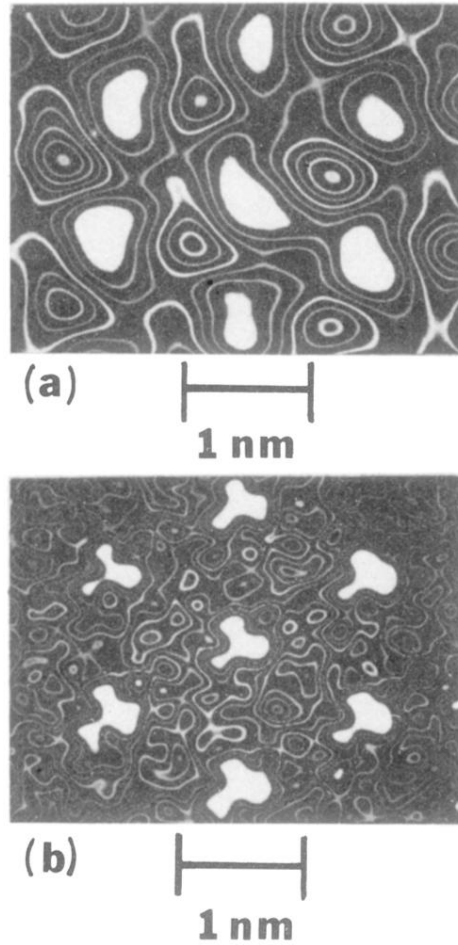


FIG. 6. (a) STM scan at 77 K from the surface of a $1T\text{-TaS}_2$ crystal presented as contours of constant z deflection (constant LDOS). Contours follow the CDW superlattice with a slight distortion by the surface S atoms. ($I=2$ nA, $V=2$ mV.) (b) In this STM scan of $1T\text{-TaS}_2$ at 77 K the contours of constant z deflection are strongly perturbed by the surface S-atom modulation. ($I=2.2$ nA, $V=2$ mV.) From Ref. 11.

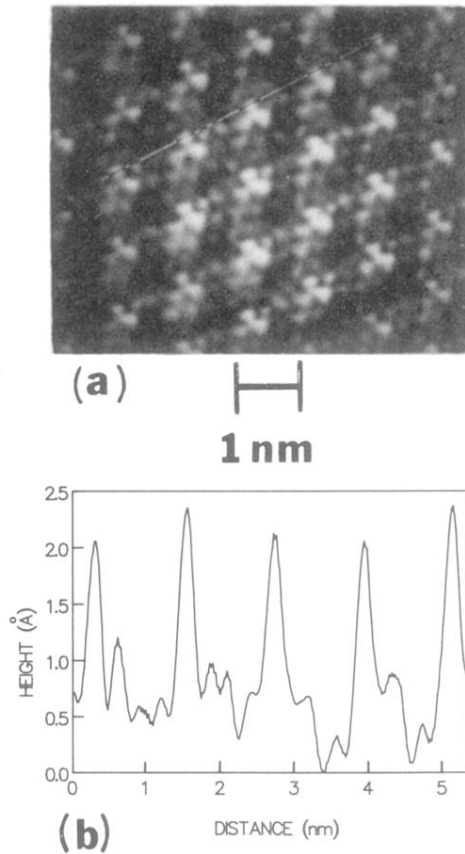


FIG. 7. (a) Gray-scale image of the STM scan on $1T\text{-TaS}_2$ at 77 K used for the contour plot in Fig. 6(b). The superimposed atomic and CDW modulations are clearly resolved with an off-center three-atom cluster marking the positions of the CDW maxima. ($I=2.2$ nA, $V=2$ mV.) (b) Profile of the z deflection along the track shown in (a). A major fraction of the deflection occurs at the CDW wavelength with a relatively small superimposed atomic modulation. From Ref. 11.

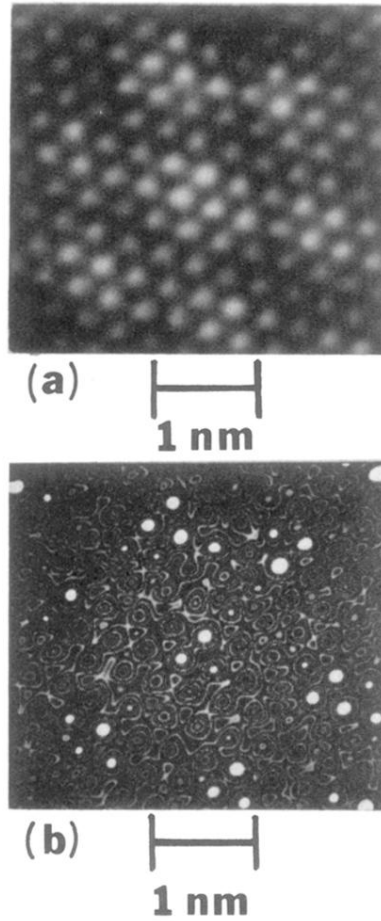
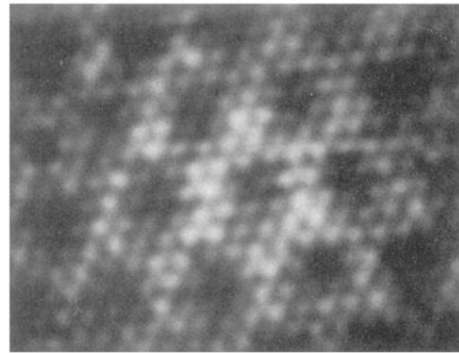


FIG. 8. (a) Gray-scale image of a STM scan on $1T\text{-VSe}_2$ at 4.2 K. The atomic and CDW modulations are of comparable magnitude. (b) Same STM scan of $1T\text{-VSe}_2$ as shown in (a) presented as contours of constant z deflection. The contours are dominated by the atomic pattern of surface Se atoms. The maxima of the CDW superlattice appear as enhanced three-atom clusters. ($I=2.2$ nA, $V=25$ mV.)




1 nm

FIG. 9. Gray-scale image of STM scan on $1T\text{-VSe}_2$ at 4.2 K. The pattern shows CDW maxima separated by rather diffuse minima instead of distinct deep minima and saddle points. This pattern is characteristic of a double- q rather than a triple- q CDW structure. ($I=2.2$ nA, $V=25$ mV.)